ENCLOSURE 2

FLN-2007-001

GNF Licensing Topical Report, "The PRIME Model for Analysis of Fuel Rod Thermal – Mechanical Performance," NEDC-33256P, NEDC-33257P , and NEDC-33258P, January 2007.

Non-Proprietary Information

IMPORTANT NOTICE

This is a non-proprietary version of Enclosure 1 to FLN-2007-001, which has the proprietary information removed. Portions of the document that have been removed are indicated by white space with an open and closed bracket as shown here [[ ]].

ENCLOSURE 2

FLN-2007-001

GNF Licensing Topical Report, "The PRIME Model for Analysis of Fuel Rod Thermal – Mechanical Performance," NEDC-33256P, NEDC-33257P , and NEDC-33258P, January 2007.

Non-Proprietary Information

IMPORTANT NOTICE

This is a non-proprietary version of Enclosure 1 to FLN-2007-001, which has the proprietary information removed. Portions of the document that have been removed are indicated by white space with an open and closed bracket as shown here [[ ]].

Global Nuclear Fuel

A Joint Venture of GE, Toshiba, & Hitachi

NEDO-33256
Class I
DRF 0000-0053-5423
January 2007

LICENSING TOPICAL REPORT

The PRIME Model for Analysis of Fuel Rod Thermal – Mechanical Performance Part 1 – Technical Bases

Disclaimer of Responsibility

This document was prepared by Global Nuclear Fuel (GNF). The use of this information for any purpose other than that for which it is intended is not authorized; and with respect to any unauthorized use, GNF makes no representation or warranty, expressed or implied, as to the completeness, accuracy or usefulness of the information contained in this document, or that its use may not infringe privately owned rights, and assumes no responsibility for liability or damage of any kind that may result from such use of this information.

Non-Proprietary Information Notice

This is a non-proprietary version of the document NEDC-33256P, which has the proprietary information removed. Portions of the document that have been removed are indicated by an open and closed bracket as shown here [[ ]].

TABLE OF CONTENTS

TABLE OF CONTENTS (continued)

LIST OF FIGURES

Global Nuclear Fuel
A Joint Venture of GE, Toshiba, & Hitachi

TABLES

SUMMARY

The PRIME model and computer program has been developed to provide best-estimate predictions of the thermal and mechanical performance of $(U,Gd)O_2$ LWR nuclear fuel rods experiencing variable power histories. The PRIME code has been developed from the GESTR-Mechanical (GSTRM) code by (1) incorporating new models to address specific high exposure mechanisms identified and quantified since the original development of GSTRM and approval of GSTRM and its associated application methodology by the NRC in 1985[1-1], (2) modifying existing material properties relations to reflect current materials properties data, including the effects of exposure where appropriate, and (3) modifying existing submodels to reflect high exposure experimental data that has become available since the original development of GSTRM.

The PRIME code addresses the effects of fuel/cladding thermal expansion, fuel phase change volume change, fuel irradiation swelling, densification, relocation and fission gas release, fuel-cladding axial slip, cladding creepdown, irradiation hardening and thermal annealing of irradiation hardening, pellet and cladding plasticity and creep, pellet hot pressing and plastic collapse, and development of a porous pellet rim at high exposure.

PRIME performs coupled thermal and mechanical interaction analyses. The incremental finite element mechanics model performs an axisymmetric radial mechanical interaction analysis to determine pellet and cladding stresses and strains at the pellet midheight location. The thermal solution is obtained by numerical evaluation of the thermal conductivity integral.

This document is Part 1 of the PRIME Licensing Topical Report (LTR) and presents the technical bases of the PRIME code and includes (1) descriptions of the technical bases for the PRIME component models and material properties relations and (2) a description of the overall structure of the PRIME model and implementation of the component models. Experimental qualification of the PRIME model by comparison of integral code predictions of fuel rod temperatures, fuel rod fission gas release and internal pressure, cladding deformations to experimental data is presented in Part 2 of this LTR (NEDO-33257) and the methodology for application of the PRIME code for licensing and design analyses is presented in Part 3 of this LTR (NEDO-33258).

1. INTRODUCTION

The PRIME model and computer program has been developed to provide best-estimate predictions of the thermal and mechanical performance of $(U,Gd)O_2$ LWR nuclear fuel rods experiencing variable power histories. The PRIME code has been developed from the GESTR-Mechanical (GSTRM) code by (1) incorporating new models to address specific high exposure mechanisms identified and quantified since the original development of GSTRM and approval of GSTRM and its associated application methodology by the NRC in 1985[1-1], (2) modifying existing material properties relations to reflect current materials properties data, including the effects of exposure where appropriate, and (3) modifying existing submodels to reflect high exposure field and experimental data that has become available since the original development of GSTRM.

New models incorporated to address specific high exposure mechanisms include development of a porous pellet rim at high exposure. Existing materials properties models modified to reflect current materials properties data include the dependency of $(U,Gd)O_2$ thermal conductivity on gadolinia; materials properties modified to reflect the effects of high exposure include $(U,Gd)O_2$ fuel thermal conductivity and (annealed) Zircaloy irradiation creep and growth. Existing submodels modified to reflect high exposure data include the pellet relocation model and the pellet fission gas release model.

The PRIME code addresses the effects of fuel/cladding thermal expansion, fuel phase change volume change, fuel irradiation swelling, densification, relocation and fission gas release, fuel-cladding axial slip and locking, cladding creep-down, irradiation hardening and thermal annealing, pellet and cladding plasticity (yield and work-hardening) and creep, pellet hot pressing and plastic collapse, and development of a porous pellet rim at high exposure. PRIME code also includes complete thermal-mechanical properties for fuel with [[ ]] additives [1-2].

PRIME performs coupled thermal and mechanical interaction analyses. The incremental finite element mechanics model performs an axisymmetric radial mechanical interaction analysis to determine pellet and cladding stresses and strains at the pellet midheight location. The thermal solution is obtained by numerical evaluation of the thermal conductivity integral.

The modifications and additions summarized above are intended to extend the capability of the PRIME code to >[[ ]] GWd/MTU peak pellet exposure, or equivalently >[[ ]] GWd/MTU rod average exposure. This document is Part 1 of the PRIME Licensing Topical Report (LTR) and presents the technical bases of the PRIME code and includes (1) descriptions of the technical bases for the PRIME component models and material properties relations and (2) a description of the overall structure of the PRIME model and implementation of the component models. Experimental qualifications of the PRIME model by comparison of integral code predictions of fuel rod temperatures, fuel rod fission gas release and internal pressure, cladding deformation to experimental data is presented in Part 2 of this LTR (NEDO-33257) and the methodology for application of the PRIME code for licensing and design analyses is presented in Part 3 of this LTR (NEDO-33258). As noted in Part 2 of the LTR, the PRIME experimental qualification data base has been greatly expanded relative to the GSTRM data base and includes a significant amount of high exposure data, including fuel temperature data, fuel rod

internal pressure data, and cladding deformation data. On the basis of the PRIME LTR, NRC approval is requested for application of the PRIME code for licensing of LWR fuel rods to a peak pellet exposure limit of [[ ]] GWd/MTU peak pellet exposure, or equivalently >[[ ]] GWd/MTU rod average exposure. In subsequent sections of this report 'exposure' and 'burnup' will be used interchangeably unless noted otherwise.

References

[1-1] Acceptance for Referencing of Licensing Topical Report NEDE-24011-P-A Amendment 7 to Revision 6, GE Standard Application for Reactor Fuel Letter, C.O. Thomas (NRC) to J. S. Charnley (GE), MFN-036-85, March 1, 1985.

[1-2] Revision 2 to Special Report MFN-170-84-0, "Fuel property and performance model revision," MFN-056-87, July 1987.

2. *PROGRAM LOGIC AND LIMITATIONS*

The PRIME code calculates fuel rod thermal and mechanical duty for variable operating power histories. The fuel rod can be modeled by up to 30 axial nodes. The fuel rod operating power history is defined by the input of the irradiation conditions for a number of time (or exposure) steps. The number of input time steps available to describe the power history is limited to 2500 at maximum.

The input fuel rod operating power history is analyzed as shown in Figure 2.1. The code performs combined incremental and iterative calculations. The input power-time steps are internally divided into smaller power increments [[ ]], and smaller time increments [[ ]]. Iterations are performed at each of these internal steps to determine gap conductance and pellet-clad interaction. The power and time increments have been set small enough to ensure convergence of the iterations. The nature of the fuel and cladding creep behavior requires small time steps after power changes when the creep rates are high but permits larger time steps later in the analysis history when the creep rates are low. The time increments employed within an input time step have been parametrically derived to ensure accurate results over the expected range of stress-strain conditions and material properties of interest in the analysis of fuel rod operation. These analysis time increments are built-in and require the size of the input time step to be less than or equal to 2000 hours.

The PRIME code performs coupled thermal and mechanical interaction analyses. The incremental finite element mechanics model performs an axisymmetric radial mechanical interaction analysis to determine pellet and cladding stresses and strains at the pellet midheight location. The thermal solution is obtained by numerical evaluation of the thermal conductivity integral.

The program flow chart (Figure 2.2) shows the sequence of calculations performed for analysis of a single time increment. First, the gas composition within the fuel rod is determined considering the initial fill gas and any fission gases released from the fuel during its irradiation history up to the present time increment. An initial estimate of the fuel rod internal gas pressure is calculated based on the gas inventory, initial fuel rod void volume, and an assumed gas temperature.

[[

]]

Figure 2.1 Schematic Representation

Next, the "axial nodes" loop is entered, wherein cladding temperatures are calculated from internally calculated cladding-to-coolant film coefficients (including the effects of input crud deposition and oxide formation on the cladding surface) and cladding thermal conductivity, or from user-specified values. This is followed by calculations to determine the extent of (l) fuel irradiation-induced densification, causing pellet radial shrinkage away from the cladding; (2) fuel irradiation swelling, either filling pellet porosity or resulting in a positive expansion of the pellet; and (3) fuel cracking and relocation, resulting in radial displacement of the cracked pellet sections toward the cladding, reducing the diametral gap.

With an assumption for the hot fuel-cladding diametral gap, the "gap conductance" loop is entered, wherein an iterative procedure is employed to calculate the pellet surface temperature using a modified version of the gap heat transfer coefficient model of Ross and Stoute[2-1]. After a converged pellet surface temperature and gap conductance is obtained for the assumed hot diametral gap, the fuel radial temperature distribution is calculated, allowing determination of the fuel thermal expansion.

[[

]]

Figure 2.2 Flow Chart for a Single Time Increment

At this point, the mechanical interaction calculations (Figure 2.3) begin. The radial thermal and mechanical calculations employ the idealization of concentrically located pellet and cladding. The effect of pellet eccentricity and/or tilting is, however, partially included through the axial slip model. The axial slip algorithm predicts the relative fuel-cladding axial strain as a function of [[ ]]. With this estimate of relative fuel-cladding axial strain, an initial estimate of the fuel and cladding total axial strain increment is made.

The simplified finite element radial mechanics analysis begins by separating the fuel rod into 3 cladding ring elements, 1 fuel-cladding gap element, and 10 fuel ring elements. The three cladding rings provide the capability to analyze nonbarrier cladding, bimetallic (barrier) cladding consisting of an outer layer of Zircaloy and an inner layer of zirconium, and trimetallic cladding consisting of an outer layer of Zircaloy, an intermediate layer of zirconium, and an inner layer of Zircaloy (Triclad^{tm} cladding). When Triclad^{tm} fuel is analyzed, all three rings are used. When barrier fuel is analyzed, the thickness of the inner ring is set to zero. When nonbarrier fuel is analyzed, the thicknesses of the two inner cladding ring elements are set to zero. The initial strain increments (treated as equivalent thermal strain increments) of each ring element due to swelling, densification, and thermal expansion are then determined. Depending upon whether the present analysis increment is a power step during an instantaneous ramp or a time step during a constant power hold, either fuel and cladding plasticity calculations or fuel and cladding creep and pellet hot pressing calculations are performed. The resultant plastic or creep strain increments are then used, together with the crack front locations determined from the previous time step, in the determination of the fuel rod element load vectors. Determination and assembly of the fuel and cladding element stiffness matrices (involving an assumption on the state of the fuel-cladding gap, i.e., open or closed), together with assembly of the element load vectors, then allows determination of the fuel and cladding ring element total strain increments.

[[

]]

Figure 2.3 Flow chart For Mechanical Interaction Model

The fuel and cladding stress components and axial loads are then determined. If the calculated fuel and cladding loads are not equal, another estimate of the fuel and cladding axial total strain increments is made and the calculations repeated until axial load equilibrium is established. At this point, the calculated fuel and cladding displacements are employed to update the fuel-cladding gap closure. If a converged thermal solution is also present at this time, the location of the fuel radial and transverse crack fronts are updated. If the thermal calculation is not converged, an iterative calculation is performed to ensure consistency between the hot fuel-cladding diametral gap calculated by the mechanical model and the hot gap employed in the gap conductance calculation. When convergence is obtained, the amount of fission gas released from the axial node is determined.

After the conditions at each axial node have been calculated, the amount of nodal fission gas release is summed axially to allow a more accurate determination of the composition of the gas occupying the fuel rod void volume. With this more precise determination of the gas composition, the entire set of calculations is repeated. This single iteration on fuel rod internal gas composition is made for each power/time increment within the input time step. However, iterations to obtain complete convergence on the internal pressure are performed for the last time increment within the input time step.

The PRIME code is considered applicable for the thermal analysis of Zircaloy-clad uranium dioxide fuel rods in light or heavy water reactors. The fuel pellets may include additions of gadolinium dioxide [[ ]] The ranges of applicability for key dimensional and performance parameters are provided in Table 2.1.

Table 2.1

LIMITS OF APPLICATION - DIMENSIONAL AND PERFORMANCE PARAMETERS

[[

]]

References

[2-1] A.M. Ross and R.L. Stoute, "Heat Transfer Coefficients Between UO_2 and Zircaloy-2," 1962 (CRFD-l075, AECL-1552).

3. FUEL ROD THERMAL MODEL

In the PRIME model, the fuel and cladding radial temperature distributions at each node are determined by performing a one-dimensional heat transfer analysis. The fuel and cladding are taken as concentric cylinders. The temperature solution begins in the coolant and progresses inward to the pellet centerline, as described below.

3.1 CLADDING TEMPERATURE DISTRIBUTION

Several options are available for determining the cladding temperature distribution. The most commonly used option calculates the cladding surface temperature based upon coolant temperature and the thermal resistances through the liquid film, crud layer and oxide layer. For Pressurized Water Reactors (PWRs), where coolant enthalpy increases without boiling, a one-dimensional axial energy balance option is available to calculate the coolant temperature at each axial node. The above options assume that the cladding is (either annealed or cold-worked) Zircaloy. For thermal simulation of instrumented experiments or where the cladding is other than Zircaloy, an option is available to input the cladding inner and outer diameter surface temperatures directly.

Values of the overall heat transfer coefficient from the coolant to cladding outer surface may be input directly for each axial node. The cladding surface temperature is then given by

$$T_{co} = T_b + \frac{q_o}{h_f} \qquad (3\text{-}1)$$

where

T_b = bulk coolant temperature (°F)

T_{co} = cladding outside surface temperature (°F)

q_o = heat flux based on initial cladding outer diameter (Btu/hr-ft^2)

h_f = input film coefficient (BTU/hr-ft^2 -°F)

Alternatively, an option is available in which the temperature drops through the liquid film, crud layer, and oxide (corrosion) layer are calculated. First, the cladding outer diameter is corrected for oxidation using the relation.

$$D'_{co} = D_{co} - 2F_{oxide}t_{oxide} \qquad (3\text{-}2)$$

where

D_{co} = initial cladding outer diameter (in)

t_{oxide} = oxide thickness (in)

F_{oxide} = ratio of reduction in clad thickness to oxide thickness

D'_{co} = cladding diameter at Zircaloy-oxide interface (in)

Two options are available for calculation of the crud and liquid film temperature drops. In the first option, temperature drops through the liquid film, crud, and oxide are calculated separately. The Jens-Lottes[3-1] equation is used for the liquid film heat transfer coefficient; the coefficient is given by

$$h_{jl} = \left(\frac{e^{P/900}}{1.9}\right)\left(q_{crud}\right)^{3/4} \tag{3-3}$$

where

P = reactor coolant pressure (psia)

q_{crud} = heat flux at crud outer surface (Btu/hr-ft^2)

and the film temperature drop is calculated as

$$\Delta T_{film} = \frac{q_{crud}}{h_{jl}} \tag{3-4}$$

The temperature drops through the crud and oxide layers are given by

$$\Delta T_{crud} = \frac{q_{crud} \times D_{crud}}{2 \times 12 \times k_{crud}} \ln\left(\frac{D_{crud}}{D_{oxide}}\right) \tag{3-5}$$

$$\Delta T_{oxide} = \frac{q_{oxide} \times D_{oxide}}{2 \times 12 \times k_{oxide}} \ln\left(\frac{D_{oxide}}{D'_{co}}\right) \tag{3-6}$$

where

D_{crud}, D_{oxide}, D'_{co} = outer diameters of crud layer, oxide layer, and clad, respectively (in)

k_{crud}, k_{oxide} = crud and oxide conductivities, respectively (Btu/hr-ft-°F)

q_{oxide}, q_{crud} = heat flux at oxide and crud outer diameters, respectively (Btu/hr-ft^2)

and

$$D_{crud} = D'_{co} + 2t_{oxide} + 2t_{crud} \tag{3-7}$$

The resulting cladding surface temperature is, therefore

$$T_{co} = T_b + \frac{q_{crud}}{h_{jl}} + \Delta T_{crud} + \Delta T_{oxide} \tag{3-8}$$

In the second option the combined temperature drop through the liquid film and the crud layer is calculated as the maximum of:

The temperature drop through the liquid film as calculated by the Jens-Lottes correlation (equation 3-3), or the temperature drop through the crud layer calculated using a crud conductivity defined by

[[ ]] (3-9)

where

[[

]]

The temperature drop through the crud then becomes

$$\Delta T'_{crud} = \frac{q_{crud} D_{crud}}{2 \times 12 \times k'_{crud}} \ln\left(\frac{D_{crud}}{D_{oxide}}\right) \tag{3-10}$$

The resulting cladding surface temperature is, therefore

$$T_{co} - T_b = [[\qquad\qquad]] \tag{3-11}$$

The above options for calculation of temperature resistances for the crud and liquid film layers primarily addess boiling conditions, under which the bulk coolant temperature remains essentially constant along the axial length of the fuel rod. The PRIME code contains an option that enables analysis of the situation in which boiling does not occur and the coolant temperature increases as it traverses the fuel rod. In this option, the coolant temperature rise is calculated explicitly using a one dimensional energy balance, evaluated at each axial node. The coolant subchannel adjacent to the fuel rod is visualized as consisting of cells through which fluid may pass in the axial direction only.

The energy balance for any cell of fluid is then

$$\dot{q}L = \dot{m}C_p\left(T_{outlet} - T_{inlet}\right) \tag{3-12}$$

where

$\dot{q}$ = linear heat generation rate (Btu/hr-ft)

L = axial node length (ft)

$\dot{m}$ = fluid mass flow rate through the cell (lbm/hr)

C_p = specific heat of the fluid (Btu/lbm °F)

T_{inlet} = coolant temperature at inlet of fluid cell (°F)

T_{outlet} = coolant temperature at outlet of fluid cell (°F)

Since the coolant inlet temperature is known, the outlet temperature may be found using the relation

$$T_{outlet} = \frac{\dot{q}L}{\dot{m}C_p} + T_{inlet} \tag{3-13}$$

and the average coolant temperature for the fluid cell is then given by

$$T_{cool} = \frac{T_{inlet} + T_{outlet}}{2}$$

For application in PRIME, the fluid mass flow rate is input. The specific heat, C_p, at each axial node is calculated as a function of the average fluid coolant temperature using the relation [3-2]

$$C_p = 0.23884\times10^{-3} FZ_1 + \frac{0.23884\times10^{-3} FZ_2}{FZ_3 - \frac{5}{9}(T_{cool} - 32)} \qquad (3\text{-}14)$$

where T_{cool} is the average coolant temperature (°F) at the node and the variables FZ_1, FZ_2, and FZ_3 are functions of pressure and obtained by linear interpolation. The values of specific heat calculated by interpolation are accurate to within ± 5% of the 1967 ASME steam tables values of C_p.

It can be shown that substituting the equation for specific heat into the equation for cell coolant outlet temperature yields a quadratic that has one real, positive root. The average coolant node temperature is then calculated as shown previously for each axial node. The remainder of the cladding surface temperature calculation for the non-boiling option is then similar to the boiling option, except as noted below.

First, the option to input the overall coolant-to-cladding outer surface heat transfer coefficient, when used in conjunction with the non-boiling option, enables direct input of the liquid film coefficient for each axial node. The cladding surface temperature is then given by

$$T_{co} = T_{cool} + \Delta T_{crud} + \Delta T_{oxide} + q_{crud}/\mathrm{FILM} \qquad (3\text{-}15)$$

where ΔT_{crud} and ΔT_{oxide} are computed per equations 3-5 and 3-6, respectively, and FILM is the user-input value of the liquid film coefficient for each axial node in Btu/hr-ft^2-°F.

Second, an option is available to calculate the liquid film heat transfer coefficient using the Dittus-Boelter correlation[3-3]; the coefficient is given by

$$h_{D-B} = \frac{k_{liq}}{D_{hyd}}\left(.023\,\mathrm{Re}^{0.8}\,\mathrm{Pr}^{0.4}\right) \qquad (3\text{-}16)$$

where

$h_{D\text{-}B}$ = Dittus-Boelter film coefficient (Btu/hr-ft^2-°F)

k_{liq} = thermal conductivity of the coolant (Btu/hr-ft-°F)

D_{hyd} flow channel hydraulic diameter (ft)

Pr = Prandtl number of the coolant

$$\mathrm{Re} = \frac{\dot{m}D_e}{A_{flow}\mu} \qquad (3\text{-}17)$$

and the equivalent diameter D_e is defined as

$$D_e = 4\frac{A_{flow}}{P_{wet}}$$

where

A_{flow} = flow area (in^2)

P_{wet} = wetted perimeter (in)

Then

$$\mathrm{Re} = \frac{\dot{m}\left(4A_{flow}/P_{wet}\right)}{A_{flow}\mu} = \frac{4\dot{m}}{\mu P_{wet}} \qquad (3\text{-}18)$$

The wetted perimeter is defined as $P_{wet} = \pi D_{crud}$. Since the dynamic viscosity (μ) is in units of lbm/ft-sec and the units of channel mass flow rate are lbm/hr, the non-dimensional Reynold's number is calculated as

$$\mathrm{Re} = \frac{\dot{m}\left(4A_{flow}/P_{wet}\right)}{A_{flow}\mu} = \frac{4\dot{m}}{\mu P_{wet}} \qquad (3\text{-}19)$$

The coolant thermal conductivity k_{liq}, Prandtl number Pr, and dynamic viscosity μ are obtained from system library programs based upon ASME results as functions of coolant temperature and pressure. The temperature rise through the liquid film is then calculated as

$$\Delta T_{film} = q_{crud} / h_{D-B} \qquad (3\text{-}20)$$

A check is performed to assure that the coolant temperature in the liquid film does not exceed the saturation temperature at that pressure $[(T_{cool} + q_{crud} / h_{D\text{-}B}) \le (T_{sat} + q_{crud} / h_{jl})]$. If this criterion is exceeded, then the Jens-Lottes film coefficient is used with T_{sat} rather than the Dittus-Boelter correlation with the node average coolant temperature.

For the boiling option, an overall heat transfer coefficient FILM based on the equation

$$\mathrm{FILM} = \frac{q_o}{\left(T_{co} - T_b\right)} \qquad (3\text{-}21)$$

is included in the program output.

The crud and oxide thicknesses can either be input at each input step, or initial values and rates of thickness increase can be input.

The cladding inside surface temperature is calculated as

$$T_{ci} = T_{co} + \frac{q_{co} D_{co} \ln(D'_{co}/D_{ci})}{2 \times 12 \times k_c} \qquad (3\text{-}22)$$

where

D_{ci} = clad inner diameter (in)

k_c = clad thermal conductivity (Btu/hr-ft-°F)

The cladding wall temperature difference is computed using values of Zircaloy and zirconium (for barrier cladding) thermal conductivities obtained from least squares fits of the data and the resulting relationship is

$$k_{clad} = B_1 + B_2 T_{ca} + B_3 T_{ca}^2 + B_4 T_{ca}^3 + B_5 T_{ca}^4 \qquad (3\text{-}23)$$

where

k_{clad} = cladding thermal conductivity (Btu/h-ft-°F)

T_{ca} = cladding average temperature (°F)

and B_1, B_2, B_3, B_4, B_5 for Zircaloy/Zirconium are

B_1 = [[
B_2 =
B_3 =
B_4 =
B_5 =]]

For simulation of other cladding types, appropriate values B_1, B_2, B_3, B_4, B_5 can be input.

For analysis of BWR fuel rods in the non-boiling region near the bottom of the rod, and specifically for determination of the film coefficient for subsequent input to analysis of the lower end plug weld, two options are available. In both options the liquid film heat transfer coefficient is calculated using the Dittus-Boelter correlation[3-3] of equation 3-16.

Then, for the first option, since the dynamic viscosity, μ, obtained from the system library programs is in units of lbm/ft-sec and the units of wetted perimeter, input as P_{WET}, and channel mass flow rate, input as $\dot{m}$, are inches and lbm/hr respectively, the non-dimensional Reynold's number is calculated as

$$\text{Re} = 4\frac{12(in/ft)}{3600(\text{sec}/hr)}\frac{\dot{m}}{\mu P_{WET}}$$

where, if the wetted perimeter is not input, the wetted perimeter is calculated using the outer diameter of the crud layer (D_{crud}) as $P_{wet} = \pi D_{crud}$.

Then

$$\text{Re} = 4\frac{12(in/ft)}{3600(\text{sec}/hr)}\frac{\dot{m}}{\pi D_{crud}\mu}$$

For the second option, the liquid film heat transfer coefficient is also calculated using the Dittus-Boelter correlation, where the channel mass flow rate is given by

$$\dot{m} = A_{flow}\ Vc\ /Sv$$

where

Vc = coolant velocity (ft/s) (input as $\dot{m}$ (m/s))
Sv = specific volume of coolant (ft^3/lbm)

Using this relation and equation 3-17, the Reynold's number is calculated as

$$\text{Re} = \frac{D_{hyd}V_C}{\mu Sv} = \frac{D_{hyd}}{12(in/ft)}\frac{\dot{m}\times 3.28084(ft/m)}{\mu Sv}$$

The coolant thermal conductivity k_{liq}, Prandtl number Pr, dynamic viscosity μ, and specific volume of coolant *Sv* are obtained from system library programs based upon ASME results as functions of coolant temperature and pressure. The temperature rise through the liquid film ΔT_{film} is then calculated using equation 3-20.

For both options, the cladding surface temperature is then given by

$$T_{co} = T_b + \Delta T_{crud} + \Delta T_{oxide} + \Delta T_{film}$$

where ΔT_{crud} and ΔT_{oxide} are temperature increases through the crud and oxide layers, computed per equations 3-5 and 3-6, respectively.

3.2 PELLET-CLADDING THERMAL CONDUCTANCE

Calculation of the fuel temperature requires knowledge of the heat transfer coefficient between the fuel pellet and the cladding. This heat transfer coefficient is calculated using a modified version of the Ross and Stoute model.[3-4]

Pellet-cladding gap conductance is assumed to be comprised of three components and given by

$$h_g = h_s + h_f + h_r \qquad (3\text{-}24)$$

where

h_g = total gap conductance (Btu/h-ft^2-°F)

h_s = heat transfer coefficient for conduction through the solid/solid contact spots (Btu/h-ft^2-°F)

h_f = heat transfer coefficient for conduction through the gas layer at the pellet-cladding interface (Btu/h-ft^2-°F)

h_r = radiation heat transfer coefficient (Btu/h-ft^2-°F)

3.2.1 Conduction Through the Solid Points of Contact

The conductance through the solid points of the contacting fuel-cladding surfaces is given by[3-4]

$$h_s = \frac{k_m P_c}{A_o \text{Hard} R_4} \qquad (3\text{-}25)$$

where

k_m = harmonic mean thermal conductivity of the fuel and the cladding (Btu/h-ft-°F)

$$= \frac{2k_{clad}\,k_{fuel}}{k_{clad} + k_{fuel}} \qquad (3\text{-}26)$$

and

k_{clad} = cladding thermal conductivity evaluated at the cladding inside surface temperature (Btu/h-ft-°F)

k_{fuel} = fuel thermal conductivity evaluated at the fuel surface temperature (Btu/h-ft-°F)

P_c = fuel-cladding interfacial pressure (psi), as calculated by the pellet/cladding mechanical interaction model

A_o = an empirically derived constant representing the mean radius of the contact spots = [[ ]] (See Reference 3-6)

Hard = Meyer hardness of the cladding inner surface (psi)

and

$$R_4 = \left[\frac{R_1^2 + R_2^2}{2}\right]^{1/4} \qquad (3\text{-}27)$$

In this equation, R_1 and R_2 are the roughness heights of the cladding inside and fuel outside surfaces in feet, respectively, and R_4 has the units of (ft $^{1/2}$).

The relationship between Meyer hardness and yield stress (YS in psi) is assumed to be given by [3-5][3-6]

$$\text{Hard} = [[\qquad\qquad]] \qquad (3\text{-}28)$$

For nonbarrier and Triclad^{tm} cladding, the cladding inner surface is Zircaloy. For barrier cladding, the inner surface is zirconium. The appropriate yield stress is used in Equation (3-28).

3.2.2 Conduction Through the Gas

The contribution to the fuel-cladding gap heat transfer coefficient due to conduction through the gas occupying the voids between solid/solid contact points is given by

$$h_f = [[\qquad\qquad]] \tag{3-29}$$

where

h_f = gap heat transfer coefficient due to gas conduction (Btu/h-ft^2-°F)

k_{fm} = thermal conductivity of the gas mixture occupying the voids between the fuel and cladding (Btu/h-ft-°F)

C = dimensionless constant related to the contact pressure to account for surface waviness and shape deviations. The dependence of the parameter C on the contact pressure is taken as

$$C = 2.75 - 1.75 \frac{P_c}{P_y} \tag{3-30}$$

with the restriction that C cannot be less than 1.0.

P_c = fuel-cladding interfacial pressure (psi)

Py = fuel-cladding contact pressure corresponding to the onset of cladding yielding, approximated by the elastic solution

$$Py = \frac{\sigma_y t}{r} = 2YS \frac{(D_{co} - D_{ci})}{(D_{co} + D_{ci})} \text{ (psi)} \tag{3-31}$$

R_l, R_2 = surface roughness of the cladding inside and fuel outside surfaces, respectively (ft)

g_r = hot pellet-cladding radial mechanical gap ($g_r \geq 0$) (in)

(g_1+g_2) = temperature jump distance for the gas occupying the fuel cladding voids (ft). This term accounts for the fractional exchange of energy of individual gas molecules with the solid surfaces.

[[

]]

The thermal conductivity of the gas at the fuel-cladding interface is a function of the concentration of the initial fill gas (or refill gases for a refabricated rod), volatile gases, released fission gases, and the gas average temperature.

It is assumed that the thermal conductivity of any of the involved component gases are of the form

$$k_{f_i} = A_{v_i} T_g^{n_i} \tag{3-32}$$

where

k_{f_i} = thermal conductivity of the i^{th} gas component (Btu/h-ft-°F)

A_{v_i} , n_i = empirical constants. The numerical values are given for helium, argon, krypton, xenon, and nitrogen in Table 3.1.

T_g = the temperature of the gas in the fuel-cladding gap (°K)

$$= \frac{5}{9}\left[\frac{T_{ci} + T_{ps}}{2} + 460\right] \tag{3-33}$$

where

T_{ci} = cladding inside surface temperature (°F)

T_{ps} = pellet surface temperature (°F)

Table 3.1 GAS THERMAL CONDUCTIVITY CONSTANTS [3-7]

Gas	A_{v_i}	n_i	Molecular Weight M_i
Helium	1.445×10^{-3}	0.721	4.003
Argon	1.28207×10^{-4}	0.7715	39.944
Xenon	3.768×10^{-5}	0.791	131.30
Krypton	2.16×10^{-5}	0.954	83.80
Nitrogen	1.55×10^{-4}	0.800	28.0

The thermal conductivity of a gas mixture is taken as

$$k_{fm} = \frac{\sum_i X_i M_i^{1/3} A_{v_i} T_g^{n_i}}{\sum_i X_i M_i^{1/3}} \qquad (3\text{-}34)$$

where

k_{fm} = thermal conductivity of the gas mixture (Btu/h-ft-^{0}F)

X_i = mole fraction of the i^{th} gas component

A_{v_i} = the empirical constant of Table 3.1 for the i^{th} gas component

M_i = molecular weight of the i^{th} gas component

n_i = the empirical exponent of Table 3.1 for the i^{th} gas component

The total number of molecules (or atoms in the case of monatomic gases) of each component of the gas mixture is calculated to determine the gas component mole fraction. The number of fill gas atoms present (N_{fill}) is calculated from the fill gas pressure at room temperature and the total as-fabricated free volume in the rod

The number of fission gas atoms generated per unit volume of fuel is given by

$$n_{fg} = \alpha_f F \qquad (3\text{-}35)$$

where

n_{fg} = number of fission gas atoms generated per cc of fuel. The total inventory of fission gas atoms is assumed to be [[ ]]

α_f = number of fission gas atoms produced per fission. The assumed value for this parameter is [[ ]] atom/fission (equivalent to [[ ]] gm-moles fission gas/GWd).

F = cumulative burnup (fissions/cc of fuel)

The total number of fission gas atoms (N_{fg}) present in the fuel is determined by applying the fission gas release model to the fission gas generated at each axial node and summing over the axial nodes.

The number of molecules of the i^{th} volatile component is calculated from

$$N_{volat_i} = \left(6.0225 \times 10^{17}\right) V_{volat} W_{fuel} \frac{VF_i}{22.414} \tag{3-36}$$

where

V_{volat} = the volume of the total volatile gases per gram of fuel at standard temperature and pressure (STP) ($\mu\ell$ /gm of fuel)

W_{fuel} = rod total fuel column weight (gm)

VF_i = volume fraction of the i^{th} volatile component, as a fraction of the total volume of volatiles

The values of V_{volat}, W_{Fuel}, and VF_i are input. [[

]]

The total number of gas molecules (atoms) is given by

$$N_{TOTAL} = N_{fill} + N_{fg} + N_{HeRe} + N_{volat} \tag{3-37}$$

where N_{HeRe} is the number of helium atoms released (see Section 8.2).

The mole fraction of gas component i is then given by

$$X_i = \frac{N_i}{N_{TOTAL}} \tag{3-38}$$

To account for uncertainties in the data, a correction factor of [[ ]] is employed in the final determination of the gas thermal conductivity when summing individual components, thus

$$k_{fm} = [[\quad\quad]] \frac{\sum_i X_i M_i^{1/3} A_{v_i} T_g^{n_i}}{\sum_i X_i M_i^{1/3}} \tag{3-39}$$

Ross and Stoute[3-4] provided a mean value of the temperature jump distance ($g_1 + g_2$) for individual UO_2-Zircaloy pairs which is consistent with most of the experimental data. At a gas pressure of one atmosphere and for interfacial temperatures of 280 to 635°F, the values in Table 3.2 were obtained.

Table 3.2 GAS TEMPERATURE JUMP DISTANCES

Filler Gas	$(g_1 + g_2)_r$, cm	$(g_1 + g_2)_r$, ft
Helium	[[	
Argon		
Xenon		
Krypton		]]

For mixtures of the above gases, the value of the temperature jump distance used is obtained by weighting the temperature jump distances of the individual components by the mole fractions of the gases present, and correcting for the increased gas temperature and rod internal pressure, i.e.,

$$(g_1 + g_2) = \sum_r X_r (g_1 + g_2)_r \frac{T_{ga}}{T_r} \frac{P_r}{P} \qquad (3\text{-}40)$$

where

$(g_1 + g_2)$ = temperature jump coefficient (ft)

X_r = mole fraction of gas component r

$(g_1 + g_2)_r$ = reference temperature jump coefficient for gas component r from Table 3-2 (ft)

T_{ga} = fuel-cladding gap average temperature (°R)

T_r = reference gas average temperature = 918°R

P = rod internal gas pressure (psia)

P_r = reference gas pressure = 14.7 psia

[[

]]

3.2.3 Radiation Heat Transfer

The radiation heat transfer at the fuel-cladding interface is usually negligible for typical steady-state operating conditions. However, for a large temperature increase across the gap, the radiation contribution becomes significant. The expression used for the calculation of an effective radiation heat transfer coefficient is

$$h_r = \frac{G_{fact}\sigma_\beta \left(T_s^4 - T_c^4\right)}{T_s - T_c} \tag{3-41}$$

where

h_r = radiation heat transfer coefficient (Btu/h-ft^2-°F)

σ_β = Stefan Boltzmann constant
= 0.173×10^{-8} (Btu/h-ft^2-(°R)^4)

T_s = fuel surface temperature (°R)
= $T_{ps} + 460$

T_c = temperature at the inside diameter of the cladding (°R)
= $T_{ci} + 460$

$$G_{fact} = \frac{1}{\frac{F_{surf}}{C_{surf}}\left(\frac{1}{\varepsilon_c}-1\right)+\left(\frac{1}{\varepsilon_f}-1\right)+G_{emfc}} \qquad (3\text{-}42)$$

F_{surf} = surface area of the fuel surface (ft^2)

C_{surf} = surface area of the cladding inside surface (ft^2)

ε_c = emissivity of the hot cladding inner surface, defined as below.

For nonbarrier and Triclad[tm] cladding, the inner surface is Zircaloy with emissivity given by

ε_c	**Temperature Range**
[[	
	]]

For barrier cladding, the inner surface is zirconium with emissivity given by

ε_c	**Temperature Range**
[[	
	]]

where

T_{ci} = temperature at the inside diameter of the cladding (°F)

G_{emfc} = a geometrical factor (which is equal to 1 for infinite planes)

ε_f = emissivity of the hot surface of the fuel
= [[ ]] (see Reference 3-12)

T_{ps} = fuel pellet surface temperature (°F)

The cladding emissivity correlations reflect emittance measurements on oxidized Zircaloy and zirconium as reported in References 3-13 and 3-14. The fuel emissivity function is a correlation of the data presented in Reference 3-15. Assuming that

$$F_{surf} \approx C_{surf}$$

equations 3-41 and 3-42 reduce to:

$$h_r = \frac{\sigma_\beta \left(T_s^4 - T_c^4\right)}{\left(T_s - T_c\right)\left(\frac{1}{\varepsilon_c} + \frac{1}{\varepsilon_f} - 1\right)} \tag{3-43}$$

3.3 FUEL TEMPERATURE DISTRIBUTION

The fuel surface temperature is calculated based on the cladding inside surface temperature and the pellet-cladding thermal conductance as

$$T_{ps} = T_{ci} + \frac{q_o \left(D_{co}/D_{ci}\right)}{h_g} \tag{3-44}$$

Iterative solution of the fuel surface temperature is required since the values of the components of the gap heat transfer coefficient are functions of the fuel surface temperature.

Temperatures at radial positions in the fuel are determined by an iterative solution to an integral form of the second order differential equation for steady-state radial heat conduction in a circular cylinder with nonuniform internal heat generation. To treat the porous pellet rim that develops at the pellet outer surface at high exposure, as discussed in Section 6.1, the rim and non-rim regions are treated separately and have different fuel densities. The pellet radial positions are determined by dividing the pellet into equal volume annular rings in each region. The rim region is divided into 2 - 10 rings and the non-rim region is divided into 4 - 40 rings. At low exposure, before development of a rim region, only the non-rim region is considered. The final number of rings in the pellet temperature calculations is dependent upon the heat flux.

Starting from the pellet outer surface, for each ring the temperature at the inner radius of the ring is calculated from the equation

$$\int_{T(J-1)}^{T(J)} K dT = F\left[R(J)\right] - F\left[R(J-1)\right] \tag{3-45}$$

where K is the thermal conductivity of the ring and is calculated as a function of temperature, exposure and porosity of the ring, $R(J)$ and $R(J\text{-}1)$ are the inner and outer normalized radii of the ring, respectively, and $T(J)$ and $T(J\text{-}1)$ are the temperatures which correspond respectively to $R(J)$ and

$R(J\text{-}1)$. In the GSTRM code, the left hand side of equation 3-45 could be integrated in closed form as

$$\int_{T(J-1)}^{T(J)} KdT = \text{[[} \qquad \text{]] (Btu/h-ft)} \qquad \text{(3-46a)}$$

where K was given by

[[ ]]

Similarly in the GSTRM code, the F-function on the righthand side of equation 3-45 could be obtained by integration of the radial power distribution. For example, for most LWR analyses, the radial power distribution in the fuel was assumed to be an n^{th} order polynomial and the F-function on the righthand side of equation 3-45 could be expressed in closed form as

$$F(\alpha) = \frac{q_o D_{co}}{12(1-\alpha_i^2)} \sum_{j=0}^{n} \frac{ZP_j}{(j+2)^2} \left[\left(1-\alpha^{j+2}\right) - (j+2)\alpha_i^{j+2} \ln\left(\frac{1}{\alpha}\right) \right] \quad \text{(Btu/h-ft)} \qquad \text{(3-46b)}$$

where

q_o	=	cladding outside surface heat flux (Btu/h-ft^2)
D_{co}	=	cladding outside diameter (in)
α_i	=	normalized inside diameter of the fuel
α	=	normalized radius
ZP_j (j=0,1, …., n)	=	constants in the polynominal describing the effective radial power distribution (including gamma-heating).

Equations 3-46a and 3-46b were substituted into Equation 3-45 and the desired temperature was determined by iteration.

For the PRIME code, the thermal conductivity model includes improved treatment of the effects of gadolinia and explicitly addresses the effects of [[ ]] additives and burnup. The resulting expression cannot be integrated in closed form, so the integration is performed numerically in the code. Similarly, a new radial power distribution option is included in the PRIME code that cannot be integrated in closed form (see Section 3.3.2), so the integration is performed numerically in the code.

3.3.1 Fuel Thermal Conductivity

In the PRIME code, the fuel thermal conductivity model is developed for UO_2 and then extended to include the effects of burnup, gadolinia and [[ ]] additive. To permit explicit treatment of the observed burnup dependency, the phonon contribution to the thermal conductivity of UO_2 is based upon the Klemens model. The burnup dependency is included by modifying the phonon term to account for the defect concentration due to burnup. The modification includes the effect of defect recovery due to thermal annealing. The gadolinia dependency is similarly addressed by additionally modifying the phonon term to account for the defect concentration due to gadolinia. Finally, the effects of addition of [[ ]] additive are explicitly addressed. The resulting fuel thermal conductivity relation is described in detail below.

3.3.1.1 UO_2-$(U,Gd)O_2$

[[

]]

The results of these tests are reflected in the PRIME code through the following thermal conductivity relations.[1]

For $T \leq T_{EUT}$

$$K = [[\qquad\qquad]] \qquad (3\text{-}47)$$

For $T > T_{EUT}$

$$K = [[\qquad\qquad]] \qquad (3\text{-}48)$$

where

K = Fuel thermal conductivity (W/mK)

[[

Global Nuclear Fuel
A Joint Venture of GE, Toshiba, & Hitachi

]] Figures 3.1 and 3.2 present a comparison of the fuel thermal conductivity for unalloyed (non-additive) UO_2 (98%TD) with 0 and 5 wt% Gd_2O_3 at 2000 and 4000 °F, respectively.

[[

]]

Figure 3.1 Fuel Thermal Conductivity for Unalloyed UO_2 at 2000 °F

[[

]]

Figure 3.2 Fuel Thermal Conductivity for Unalloyed UO_2 at 4000 °F

3.3.1.2 Defect Recovery Fraction

As noted in Section 3.3.1.1, the thermal conductivity model included in the PRIME code addresses defect recovery due to thermal annealing. [[

]]

3.3.2 Radial Power Distribution

The PRIME code contains several radial power distribution options.

In the first option, a polynominal is used to express the radial fission density distribution in UO_2 fuel pellets as a continuous function of [[

Global Nuclear Fuel
A Joint Venture of GE, Toshiba, & Hitachi

]]

Table 3 COEFFICIENTS FOR THE GENERALIZED RADIAL FISSION DENSITY DISTRIBUTION

[[

]]

A second radial power distribution option included in the PRIME code is derived from the Bessel solution to the neutron diffusion equations in the fuel, for the case when the neutron scattering cross section is much larger than the absorption cross section, and is considered applicable to fuel irradiated in heavy water reactors. The radial fission density distribution is given by

[[

]]

A third option allows input of the center-to-surface fission density ratio (FLUXD) for each axial node. This option is available for evaluating fuel rod performance of non-GNF fuel rods where enrichment or pellet geometry is significantly different from the GNF design, thereby invalidating the use of the flux depression models presented above. In this option, the radial fission density distribution is assumed to be parabolic and given by

[[(3-56)

]]

A fourth option is based upon the RADAR model.[3-15] The RADAR model describes fission density as

[[

Global Nuclear Fuel
A Joint Venture of GE, Toshiba, & Hitachi

]]

[[

]]

3.3.3 Fuel Melting

In the PRIME code, the fuel melting temperature model is developed similarly to the fuel thermal conductivity model (see Section 3.3.1). The relation for the melting temperature of UO_2 is developed and then extended to include the effects of burnup, gadolinia and [[ ]] additive, based upon thermal arrest measurement data for UO_2, $(U,Gd)O_2$ and UO_2 containing [[ ]] additive. The resulting fuel melting temperature relation is described in detail below.

[[

Global Nuclear Fuel
A Joint Venture of GE, Toshiba, & Hitachi

Global Nuclear Fuel
A Joint Venture of GE, Toshiba, & Hitachi

]]

[[

]]

Figure 3.3 Additive Fuel Phase Diagram (Schematic)

3.3.4 Grain Growth

Grain growth is given by

[[

]]

For application in the PRIME code, grain growth is calculated for each pellet ring. [[

]] No grain growth is assured when the current grain diameter is equal to or larger than [[ ]] μm.

3.3.5 Fuel Stored Energy

In the PRIME code, stored energy is calculated for each pellet ring and then weighted by the annular ring volume to obtain the pellet stored energy. For each ring the stored energy is given by

[[

Global Nuclear Fuel
A Joint Venture of GE, Toshiba, & Hitachi

]]

References

[3-1] W.H. Jens and P.A. Lottes, "Analysis of Heat Transfer, Burnout, Pressure Drop, and Density Data for High Pressure Water," USAEC Report, 1951 (ANL-4627).
[3-2] E. Schmidt, "Properties of Steam and Water", (1969).
[3-3] F.W. Dittus and L.M.K. Boelter, University of California, Berkeley, Publ. Eng., 2, 433 (1930).
[3-4] A.M. Ross and R.L. Stoute, "Heat Transfer Coefficients Between UO_2 and Zircaloy-2," 1962 (CRFD-1075, AECL-1552).
[3-5] G.E. Dieter, "Metallurgy and Metallurgical Engineering Series", McGraw-Hill, New York, 1961.
[3-6] I.D. Peggs, et. al., "The Yield Strength-Hot Hardness Relationship of Zircaloy-4", J. Nuclear Mat'ls., 57, (1975), pp. 246-248
[3-7] H. Von Ubish, S. Hall, and R. Srivastav, "Thermal Conductivities of Mixtures of Fission-Product Gases with Helium and with Argon," U.N. International Conference Peaceful Uses of Atomic Energy, A/conference 15/P/143, Sweden (1958).
[3-8] Burgoyne and Garlick at the OECD-CSNI meeting on the Behavior of Water Reactor Fuel Elements under Accident Conditions in Spinad, Norway on September 13-16, 1976.
[3-9] F. Cabannes, J.P. Stora, and J. Tsakiris, "Reflectivity and Emissivity of UO_2 at High Temperatures," Gomptes Rendus Academy of Science, Paris, 264, Series B, p. 45-48 (January 4, 1967).
[3-10] M. Amaya, et al., "Thermal Conductivities of Irradiated UO_2 and $(U,Gd)O_2$ Pellets", J. Nucl. Mater. 300, (2002) 57.
[3-11] S. Ishimoto, et al., "Efects of Soluble Fission Products on Thermal Conductivities of Nuclear Fuel Pellets", J. Nucl. Sci. Technol., 31[8], (1994) 796.
[3-12] M. Hirai et al, 'Thermal Diffusivities and Thermal Conductivities of UO_2-Gd_2O_3', J. Nucl. Science and Tech., Vol. 28, Nov. 1991.
[3-13] "Assessment of Recent Data and Correlations for Fuel Pellet Thermal Conductivity", Paper F1.1, EPHG Meeting, March 2001.
[3-14] P. Lucuta et al, Proc. 2nd Int. Conf. CANDU Fuel, Ontario, Canada, October 1989.
[3-15] I.D. Palmer, K.W. Helketh and P.A. Jackson, "Water Reactor Fuel Element Computer Modelling", Ed. by G. Gittus, p.321, Applied Science Publishers (1983).
[3-16] K. Kogai, R. Iwasaki and M. Hirai, "In-Pile and Out-of-Pile Grain Growth Behavior of Sintered UO_2 and $(U,Gd)O_2$ Pellets, J. Nucl. Sci. Tech., 26, 744-751 (1989).

4. MATERIAL PROPERTIES

4.1 CLADDING ELASTIC/PLASTIC PROPERTIES

4.1.1 Elastic Modulus

The elastic modulus of Zircaloy cladding and zirconium barrier is given by

$$E_c = [[\qquad\qquad]] \tag{4-1}$$

where

E_c = cladding elastic modulus (psi)

T_{ca} = cladding average temperature (°F)

The equation presented above represents an average of anisotropic relations for Young' s modulus of LWR tubing in the hoop and axial directions. This average is used to provide an effective "isotropic" relation required by the mechanics model mathematical formulation. The anisotropic Young's modulus relations were derived analytically using LWR zircaloy tubing x-ray texture measurements and zirconium single crystal elastic constant measurements reported in References 4-1 and 4-2. The values derived by this method have been verified by comparison to measurements of Young's modulus in the axial direction reported in References 4-3 and 4-4.

4.1.2 Poisson's Ratio

The cladding/barrier Poisson's ratio is given by

$$\nu_c = [[\qquad\qquad]] \tag{4-2}$$

where

ν_c = cladding Poisson's ratio

T_{ca} = cladding average temperature (°F)

This correlation has been derived analytically from extensive x-ray texture measurements on Zircaloy tubing and zirconium monocrystal elastic constants.

4.1.3 Yield Stress and Hardening Rule

In the plastic regime, the relationship between (uniaxial) true stress and (uniaxial) true strain for cold worked and annealed Zircaloy and zirconium is similar to that used in MATPRO Version 11 and given by

$$\sigma = [[\qquad\qquad]] \tag{4-3}$$

where

σ = stress (psi)

ε_p = permanent strain (in/in)

$\dot{\varepsilon}$ = strain rate (in/in-hr)

and

K = strength coefficient

n = strain hardening exponent

m = strain rate sensitivity exponent

In the PRIME code, the value of $\dot{\varepsilon}$ is input to simulate fast loading; the value used is [[ ]] in/in-hr.

The strength coefficient K is given by

$$K = \min(K^{high}, K^{low}) \tag{4-4}$$

In this equation, K^{high} is the coefficient determined from high temperature data and K^{low} is the coefficient determined from low temperature data (<450°C).

At low temperature (<450°C), the strength coefficient is given by

$$K^{low} = [[\qquad\qquad]] \tag{4-5}$$

where

For Annealed Zircaloy

$J = [[$]]

$Z = [[$]] $\psi \le 3.5\times10^{21}$

$= [[$]] $\psi > 3.5\times10^{21}$

For Cold-Worked Zircaloy

$J = [[$]]

$Z = [[$]] $\psi \le 3.5\times10^{21}$

$= [[$]] $\psi > 3.5\times10^{21}$

For Zirconium

$J = [[$]]

$Z = [[$]] $\psi \le 3.5\times10^{21}$

$= [[$]] $\psi > 3.5\times10^{21}$

and

$R = [[$]] (4-6)

where

T = temperature (°C)

ψ = fast neutron fluence (n/cm^2 > 1MeV)

In the expression for K, J accounts for the temperature dependence, Z accounts for the fast-neutron fluence dependence, and R accounts for temperature annealing effects.

[[

]]

The plasticity relations presented above apply for cladding temperatures up to ~1100°F.

4.2 ANNEALING OF IRRADIATION HARDENING

In most applications of the PRIME code, the temperature varies with time. Generalization of the relations for plasticity and yield stress (Section 4.1) and thermal creep (Section 4.4) for such applications is discussed below.

The effects of concurrent hardening and annealing appear implicitly in the values of strength coefficient K and strain hardening exponent n, and can be modeled as functions of temperature and time[4-5][4-6][4-7][4-8]. From Section 4.1 the definitions of n and K are

[[

]]

[[

]]

Figure 4.1 Hardening Group Approximation to Retained Hardening Function

[[

]]

4.3 FUEL DENSITY

The theoretical density of $(U,Gd)O_2$ [[ ]] additive fuel is given by [[

]] (4-17)

4.4 FUEL ELASTIC/PLASTIC PROPERTIES

4.4.1 Modulus of Elasticity

Based upon the (generally) assumed temperature dependence of the modulus of elasticity (Young's modulus) of ceramic oxides with 100% theoretical density (TD) and the theoretical formulation for the impact of porosity on the elastic modulus of ceramic oxides,[4-9][4-10] in the PRIME code the fuel modulus of elasticity is taken as

$$E_U = [[\quad]] \quad (4\text{-}18)$$

where

E_U = local fuel elastic modulus (psi)

T_k = local fuel temperature (K)

ρ = initial pellet density (%TD)

[[

]]

4.4.2 Poisson's Ratio

The fuel Poisson's ratio is given by

$$\nu_f = [[\qquad\qquad\qquad\qquad]]$$

where

ν_f = fuel Poisson's ratio

ρ = initial pellet density (%TD)

4.4.3 Yield Stress

[[

]] Based upon the results, the fuel yield stress in the PRIME code is given by

[[

]]

4.4.4 Strain Hardening Coefficient and Tangent Modulus

In the PRIME code, the fuel material stress-strain curve is given by the relation

[[

]] (4-24)

4.4.5 Plastic Poisson's Ratio

In general, plastic deformation is assumed to be nondilatational, i.e. plastic deformation does not include an associated volume change. In the PRIME code, this assumption is applied [[

]]

References

[4-1] E.S. Fisher, C.J. Renken, "Adiabatic Elastic Moduli of Single Crystal Alpha Zirconium," J. Nuclear Mat'ls., 4 (1961) pp. 311-315.
[4-2] E.S. Fisher, C.J. Renken, "Single Crystal Elastic Moduli and the hcp bcc Transformation in Ti, Zr, and Hf," Phys. Dev., 135 (1964), AA82-AA94.
[4-3] D.O. Northwood, et. al, "Elastic Constants of Zirconium Alloys," J. Nuclear Mat'ls., 55, (1975) pp. 299-310.
[4-4] D.O. Northwood, H.E. Rosinger, "Influence of Oxygen on the Elastic Properties of Zircaloy-4," J. Nuclear Mat'ls., 89, (1980), pp. 147-154.
[4-5] A.A. Bauer, et. al., "Evaluating Strength and Ductility of Irradiated Zircaloy, Task 5," Quarterly Progress Report January/March 1978 (NUREG/CR-0085 BMI-2000).
[4-6] D.L. Hagerman, "Effects of Annealing of Irradiation Damage and Cold Work on Cladding Plastic Deformation," USNRC, October 1977 (TFBP-TR-207).
[4-7] G.J.C. Carpenter and J.F. Watters, "Irradiation Damage Recovery in Some Zirconium Alloys," Zirconium in Nuclear Applications, American Society for Testing and Materials, 1974, ASTM STP 551, pp. 400-415.
[4-8] C.J. Baroch, A.V. Munim, and E.N. Harbinson, "Effects of Irradiation in a Thermal Reactor on the Tensile Properties of Zircaloy 2 and 4 and Borated Stainless Steel," Irradiation Effects on Structural Alloys for Nuclear Applications, American Society for Testing and Materials, 1970, (ASTM STP 484), pp. 176-193.
[4-9] J.B. Wachtman, et. al., "Exponential Temperature Dependence of Young's Modulus for Several Oxides," Phys, Rev. 122, 1754-1759, 1961.
[4-10] O.L. Anderson, "Derivation of Watchman's Equation for the Temperature Dependence of Elastic Modulus of Oxide Compounds," Phys. Rev. 144, 553-557, 1966.
[4-11] K.C. Radford and G.R. Terwilliger, "Compressive Deformation of Poly-crystalline UO_2", J. American Ceramic Soc., 58, 7-8, 1975.

5. FUEL AND CLADDING EXPANSION/DISPLACEMENT MODELS

After determination of the fuel and cladding temperatures, as described in Section 3, the (hot) fuel pellet-cladding interaction state is determined using a finite element based mechanics solution. The finite element and the incremental compliance matrix used in the solution are derived in Appendices A and B, respectively. The interaction state is either an open gap of a specific magnitude or a closed gap with a specific pellet-cladding interface pressure. Inputs to the mechanics solution include fuel and cladding equivalent strain increments resulting from (l) fuel and cladding thermal expansion, (2) cladding irradiation growth, (3) fuel irradiation swelling, (4) irradiation-induced fuel densification, (5) fuel relocation, (6) fuel and cladding creep, and (7) fuel hot pressing. The extent of relative fuel-cladding axial expansion (axial slip strain) also contributes to the determination of the hot fuel-cladding gap state.

5.1 FUEL AND CLADDING THERMAL EXPANSION

For Cladding

In the PRIME code, the Zircaloy and zirconium (for barrier cladding and Triclad [tm] cladding) elements of the cladding are modeled separately. The thermal expansions of both Zircaloy and zirconium are given by

$$\alpha_i = \alpha_c \ (f_i) \ + \ \alpha_a \ (1 - f_i)$$

where

α_i = coefficient of cladding thermal expansion for direction *i*

f_i = cladding basal pole texture factor in direction *i*

α_c = zirconium single crystal coefficient of thermal expansion in the unit cell *c*-axis direction

α_a = zirconium single crystal coefficient of thermal expansion in the unit cell *a*-axis direction

and

$$a_{c_r} = [[\qquad]] \qquad (5\text{-}1)$$

$$a_{c_\theta} = [[\qquad]] \qquad (5\text{-}2)$$

$$a_{c_z} = [[\qquad\qquad]] \tag{5-3}$$

where

α_{c_r} = cladding thermal expansion coefficient in the radial direction (in/in-°F)

α_{c_θ} = cladding thermal expansion coefficient in the circumferential direction (in/in-°F)

α_{c_z} = cladding thermal expansion coefficient in the axial direction (in/in-°F)

The values for α_c and α_a include the temperature dependence indicated in References 5-1 and 5-2.

The thermal expansion equivalent strain is then given by

$$\varepsilon_{t_i} = \alpha_{c_i}\left(T_{ca} - 68\right) \tag{5-4}$$

where

ε_{t_i} = cladding thermal strain in direction *i* (in/in)

α_{c_i} = cladding thermal expansion coefficient in direction *i* (in/in °F)

<u>For Fuel</u>

The thermal expansion equivalent strain of a fuel pellet ring is assumed isotropic and given by

[[

Global Nuclear Fuel
A Joint Venture of GE, Toshiba, & Hitachi

]]

5.2 CLADDING IRRADIATION GROWTH

The irradiation growth relation for annealed Zircaloy cladding is

[[

]] (5-8)

5.3 FUEL IRRADIATION SWELLING

The accumulation of fission products leads to volumetric expansion of the fuel material. This expansion is offset to varying degrees by closure of pores within the fuel. Small pores close at a rapid rate early during irradiation through irradiation enhanced vacancy diffusion. Rapid closure of pellet porosity by this mechanism is treated by a separate irradiation-induced densification model. Longer term closure of pellet porosity can be accomplished either by hot pressing of the fuel material under a compressive stress state or by the accumulation of fission products causing an irradiation-induced swelling of the fuel material. Volumetric strains attributed to irradiation swelling are the net dimensional changes resulting from the fission product accumulation volumetric expansion minus the corresponding changes due to long-term closure of pellet porosity.

Analytically, fission product swelling is divided into two components. The first, called external swelling, is the component of swelling that gives external dimensional changes throughout life. The second, called internal swelling, is the remaining component that is offset by long-term closure of pellet porosity and that contributes to external dimensional changes only after pellet porosity is closed.

The total swelling ($\Delta V_S/V$) is given by

$$\frac{\Delta V_S}{V}=\frac{\Delta V_{SP}}{V}+\frac{\Delta V_{SE}}{V} \qquad (5\text{-}9)$$

where

$$\frac{\Delta V_{SP}}{V} = [[\quad]]$$

$$\frac{\Delta V_{SE}}{V} =$$

and

α_ρ = internal swelling rate ($\Delta V/V$ per 10^{20} f/cc)

α_E = external swelling rate ($\Delta V/V$ per 10^{20} f/cc)

ρ = initial pellet density (%TD)

$\Delta\rho_D$ = pellet density increase due to irradiation-induced densification (% TD)

$\Delta\rho_{HP}$ = pellet density increase due to hot pressing (% TD)

F = cumulative exposure (f/cc), defined as:

$F =$ [[

$\times$

$=$

]]

where

E = fuel exposure (MWd/MTU)

ρ_{th} = fuel theoretical density (gm/cc) (see equation (4-16) in Section 4.3)

G = gadolinia concentration (wt % Gd_2O_3)

A = additive concentration (wt %)

Pellet porosity is defined, in volume percent, by 100 x $\left[1-\frac{\rho_c}{\rho_{th}}\right]$, where ρ_c is the calculated pellet density at the current time. The calculation of ρ_c includes changes in density due to in-reactor densification and hot pressing. [[

]].

[[

]]

5.4 FUEL DENSIFICATION

The model for the kinetics of the volume-diffusion-controlled densification process is modified to exclude fuel irradiation swelling, as the swelling component is considered separately, as discussed in the preceeding section. The resulting expression for the density change due to in-reactor densification is

[[

]]

5.5 FUEL RELOCATION

During the initial rise to power, the steep fuel pellet radial temperature gradient causes radial cracking in the fuel at very low power levels. When this cracking occurs, the resulting fragments move radially outward toward the cladding, resulting in initial fuel relocation. The initial relocation is modeled such that the fuel pellet forms a number of [[

Global Nuclear Fuel

A Joint Venture of GE, Toshiba, & Hitachi

Global Nuclear Fuel

A Joint Venture of GE, Toshiba, & Hitachi

]]

[[

]]

Figure 5.1 Schematic Representation of Initial Fuel Relocation

[[

]]

[[

]]

Figure 5.2 Idealization of Relocation as Translation of Displaced Node NF

[[

Global Nuclear Fuel
A Joint Venture of GE, Toshiba, & Hitachi

]]

5.6 CLADDING AND BARRIER CREEP

The relations describing creep of recrystallized Zircaloy and zirconium depend upon the stress regime. For constant stress and temperature, creep in the low and intermediate stress regimes is given by

[[

Global Nuclear Fuel
A Joint Venture of GE, Toshiba, & Hitachi

]]

5.6.1 Low Stress Regime

For the low stress regime, defined approximately as [[

]]

5.6.2 Intermediate Stress Regime

For the intermediate stress regime, defined approximately as [[

=

]]

5.6.3 High Stress Regime

In the high stress regime, defined approximately as [[

]]

5.6.4 Thermal Annealing

[[

]]

5.6.5 Cladding Creep Rate

[[

]]

5.6.6 Principal Creep Components

[[

]]

5.7 FUEL CREEP

Uniaxial compression tests have been performed to determine the creep characteristics [[

]]

The results of these tests are reflected in the PRIME model through the use of a fuel pellet creep model of the form

[[

Global Nuclear Fuel
A Joint Venture of GE, Toshiba, & Hitachi

Global Nuclear Fuel

A Joint Venture of GE, Toshiba, & Hitachi

]]

5.8 FUEL HOT PRESSING

In a porous medium, such as a fuel pellet, the development of a stress field provides the potential for a mechanical densification, or removal of porosity, by material creep.

[[

Global Nuclear Fuel
A Joint Venture of GE, Toshiba, & Hitachi

]]

5.9 FUEL-CLADDING AXIAL SLIP

The basic thermal and mechanical calculations idealize the pellet and cladding as concentric cylinders. A potential effect of pellet eccentricity and/or tilting is to promote axial fuel column locking, resulting in greater fuel radial and cladding axial expansion. In the thermal solution no account is directly taken for the effects of pellet eccentricity or tilting. However, the mechanics solution does address these pellet stacking effects through the use of a fuel-cladding axial slip strain, defined as the difference between the pellet axial total strain and the cladding axial total strain.

[[

Global Nuclear Fuel

A Joint Venture of GE, Toshiba, & Hitachi

]]

References

[5-1] D.L. Douglass, "The Metallurgy of Zirconium," Atomic Energy Review, Supplement 1971, Vienna 1971.
[5-2] B. Lustman, F. Kerze Jr., "The Metallurgy of Zirconium," McGraw-Hill, 1955.
[5-3] J.B. Conway, et. al., "The Thermal Expansion and Heat Capacity of UO_2 to 2200°C," Trans ANS.6. No. 1, June 1963.
[5-4] J.A. Christensen, "Thermal Expansion and Change in Volume of Uranium Dioxide on Melting," October 1962 (HW-75148).
[5-5] R.A. Morgatroyd, A. Rogerson, "An Assessment of the Influence of Microstructure and Test Conditions on the Irradiation Growth Phenomenon in Zirconium Alloys," J. Nuclear Mat'ls, 90, (1980), pp. 240-248.
[5-6] Solomon et al, 'Fission Induced Creep of UO_2 and Its Significance to Fuel Element Performance', ANL-7857, Argonne National Laboratory, Sep. 1971.
[5-7] Revision 2 to Special Report MFN-170-84-0, "Fuel property and performance model revision," MFN-056-87, July 1987.

6. HIGH BURNUP MODELS

The major objectives for development of the PRIME model are (1) to address high burnup phenomena and mechanisms that have been identified and quantified subsequent to the development and qualification of the GSTRM code (in 1984) and (2) thus better predict high burnup fuel performance experimental data that has become available through GNF and industry experimental programs since 1984.

As noted in Section 1, the PRIME model has been developed from the GSTRM model. The approach was to (1) modify material properties used in GSTRM to include exposure dependencies or to modify existing dependencies on the basis of available properties data, (2) modify exposure dependencies in burnup dependent GSTRM submodels and incorporate new submodels to address high exposure phenomena and mechanisms not already addressed, and (3) modify specific GSTRM submodels to address an expanded experimental database including high burnup fuel centerline temperature data, fission gas release data, and cladding deformation data.

The major change in material properties is to include an explicit exposure dependency in the fuel thermal conductivity, as indicated by results of fuel irradiation programs and laboratory measurements. Other changes include modified irradiation growth for annealed Zircaloy to reflect observed acceleration in growth at high fluence (burnup) and modified creep for annealed Zircaloy to reflect new data for BWR operating conditions. Changes to submodels include addition of a new fuel radial power distribution option with explicit exposure dependency at high burnup (the GSTRM exposure dependency assumed saturation at [[ ]] GWd/MTU) and incorporation of a model to address the observed development of a porous pellet rim at high burnup. Specific submodels modified to better predict high exposure experimental data include the fuel pellet relocation and recovery model and the fission gas release model.

With the exception of the model for development of the porous pellet rim, the modifications and additions noted above are described in detail in other sections of this report. The model for development of the porous rim is described below.

6.1 DEVELOPMENT OF POROUS PELLET RIM AT HIGH EXPOSURE

It is known that a porous rim structure is formed in high burn up pellets. The PRIME model takes into account the effects of rim structure by addressing the effects of increased porosity (and corresponding decreased density). An increase of pellet porosity results in a decrease of pellet thermal conductivity and an increase of pellet volume.

[[

Global Nuclear Fuel
A Joint Venture of GE, Toshiba, & Hitachi

]]

[[

]]

Figure 6.1 Rim Growth

[[

]]

Figure 6.2 Porosity at the Rim Region

Global Nuclear Fuel

A Joint Venture of GE, Toshiba, & Hitachi

[[

Global Nuclear Fuel
A Joint Venture of GE, Toshiba, & Hitachi

]]

7. MECHANICS MODEL

During the initial rise to power, fuel pellets develop radial and transverse cracks. These cracks initiate at very low power levels where the pellet temperatures are low and the pellets are brittle over their entire cross section. Consequently, these initial cracks most likely extend to the pellet centerline as a result of dynamic propagation. Subsequent power cycling results in intermittent radial and axial interaction between fuel and cladding. The radial interaction is primarily a result of differential expansion between pellet and cladding. The axial interaction is primarily a result of friction buildup or "locking" due to the stochastic distribution of pellets within the cladding, and can occur even without hard radial contact.

The PRIME code performs coupled thermal and mechanical interaction analyses. The thermal solution is discussed in Section 3. The purpose of this section is to describe the treatment of the preceding effects in the fuel rod mechanical analysis.

7.1 GEOMETRIC MODEL

The fuel rod is pictured as a number of identical right circular pellets stacked concentrically in a straight circular cladding. During the initial rise to power, the pellets develop a number of equally spaced radial and traverse cracks, as shown schematically in Figure 7.1. [[

]]. The number of cracks is assumed to be fairly large, but does not appear explicitly in the mechanics model. The effect of the number of cracks on the accuracy of the mechanics model is discussed elsewhere in this report.

[[

]]

Figure 7.2 Segment of Fuel Rod Modeled by Code

The pellet is divided into [[ ]] rings of equal thickness (the mechanical impact of the porous pellet rim is addressed by the additional swelling described in Section 6.1). Each ring is modeled by a finite element. [[

]]

The element assignment is summarized in the table below.

Element Number*

[[

]]

In the mechanics model, initial pellet cracking is assumed to occur when the normal stress in the circumferential or axial direction at any radial position exceeds [[

]]

The mechanics model considers the effects of both radial and axial interactions, and the Poisson's coupling between the two. Radial interaction is simulated using a gap element, which has negligible radial stiffness when the gap is open and infinite stiffness when the gap is closed. [[

]]

[[

]]

Figure 7.3 Pellet Cladding Diffferential Axial Strain (Schematic)

7.2 MATHEMATICAL MODEL

Mathematically, the mechanics model is based upon the finite element technique.[7-1][7-2] The fuel rod segment included in the model is reduced to a mathematical model with a finite number of degrees of freedom. Equilibrium equations for the model are obtained by minimizing the potential energy of the finite element system. The results are equivalent to those that would be obtained using the classical Ritz sequence method.

The input power history consists of a series of instantaneous power changes and constant power hold periods. Incremental constitutive relations for both pellet and cladding, based upon (instantaneous) plasticity theory and developed within the finite element framework are used during the power changes; an initial strain approach for creep, based upon equation-of-state creep relations and consistent with the incremental plasticity formulation, is used during constant power operation.

[[

]]

]]

Figure 7.4 Ring Element

[[

]]

Global Nuclear Fuel

A Joint Venture of GE, Toshiba, & Hitachi

Global Nuclear Fuel
A Joint Venture of GE, Toshiba, & Hitachi

]]

[[

]]

Figure 7.5 Geometric Model for Fuel Rod Cross Section

[[

]]

7.3 INCREMENTAL CONSTITUTIVE RELATIONS

[[

Global Nuclear Fuel

A Joint Venture of GE, Toshiba, & Hitachi

Global Nuclear Fuel
A Joint Venture of GE, Toshiba, & Hitachi

]]

[[

]]

Figure 7.6 Time Hardening and Strain Hardening for Creep

[[

]]

[[

]]

Figure 7.7 Definition of Strain Increment

[[

Global Nuclear Fuel

A Joint Venture of GE, Toshiba, & Hitachi

Global Nuclear Fuel
A Joint Venture of GE, Toshiba, & Hitachi

]]

7.4 PELLET CRACKING AND REDUCED CONSTITUTIVE RELATIONS

[[

]]

[[

]]

Figure 7.8 Definition of Tangent Modulus

[[

Global Nuclear Fuel

A Joint Venture of GE, Toshiba, & Hitachi

Global Nuclear Fuel

A Joint Venture of GE, Toshiba, & Hitachi

Global Nuclear Fuel
A Joint Venture of GE, Toshiba, & Hitachi

]]

7.5 INCORPORATION OF GROWTH MODELS INTO MECHANICS MODEL

In operating fuel rods, there are mechanisms that can change the dimensions of the pellets and cladding. These mechanisms occur in addition to thermal expansion and creep and are denoted growth mechanisms. The growth mechanisms considered for the pellet include:

a. Relocation
b. Swelling
c. Densification
d. Volume change due to phase changes when melting or resolidification occurs

The single growth mechanism considered for the cladding is irradiation-induced growth.

The growth mechanisms, except relocation, are incorporated into the PRIME mechanical model through the constitutive relations (Equation 7-5). The component growth models of Section 5 predict the incremental growth in each of the principal directions resulting from the growth mechanisms as functions of parameters such as fluence, temperature, or state of stress. These incremental growths, with the exception of relocation, are transformed to incremental strains and included in the vector $\Delta\varepsilon^{I}$ of initial strain increments, as discussed in Section 7.3.

The growth mechanisms do not directly change the stress state in an unconstrained fuel pellet, or in an empty fuel rod. Pellet growth is therefore applied uniformly to the ten ring elements. The resulting fuel and cladding strains/displacements do, however, affect the degree of pellet-cladding interaction and by this means, the growth mechanisms affect the stress state of the fuel rod.

7.6 CLAD THICKNESS REDUCTION DUE TO OXIDE FORMATION

Fuel rod operation at cladding temperatures typical of commercial LWRs results in partial cladding oxidation (on the outer surface) with a resulting reduction in cladding thickness. The oxide thickness increases and the cladding thickness decreases with continued operation. The effect of cladding oxide formation on cladding surface temperature and temperature drop across the cladding is treated directly (see Section 3.1). The impact of cladding oxide formation on cladding stresses and strains is addressed as follows.

The cladding hoop and axial stress increments are calculated for each loading increment using the finite-element mechanics model. The effect of reduced cladding thickness due to oxide formation is included in the calculation by using the current cladding outside diameter D'_{Co} for each incremental calculation and by applying radial and axial loading increments equal to the product of the hoop and axial stresses at the start of the increment and the reduction in cladding thickness from the prior increment due to oxide formation.

7.7 PELLET-CLADDING INTERACTION

The mechanics and thermal models are coupled through the pellet-cladding gap conductance model. The gap conductance is a function of the pellet-cladding diametral interaction, I. The (current) value of I is a function of the current pellet and cladding radial displacements and the initial (as-fabricated) pellet-cladding gap and is given by the relation

$$I = 2\left(u_r^c - u_r^p + \frac{G_o}{2} \right) \tag{7-34}$$

where

u_r^p = Current radial displacement (relative to manufactured geometry of rod) of pellet outer surface

u_r^c = Current radial displacement (relative to manufactured geometry of rod) of cladding inner surface

G_o = as-manufactured pellet-cladding diametral gap

The pellet radial displacement includes the effects of pellet relocation. [[

]]

[[

]]

Figure 7.9 Pellet Surface After Initial Relocation

[[

]]

7.8 LOSS OF INITIAL PELLET DISHING

In many fuel designs, the pellet is manufactured with a shallow dish at one or both ends, as shown schematically in Figure 7.10(a). During operation of the fuel, plastic flow, creep, and/or hot pressing of the pellet into the dish volume may occur, resulting in lower pellet-cladding interface pressures and lower cladding hoop strains and stresses. However, such response results in a permanent loss of the dish volume, which in turn changes the distribution of volume available to accommodate released fission gas.

The initial dish geometry is described by specifying an average dish depth, x_i, for each ring element, as shown schematically in Figure 7.10(b). During the operating history, x_i is permitted to decrease as dictated by the current state of stress in the pellet until it becomes zero.

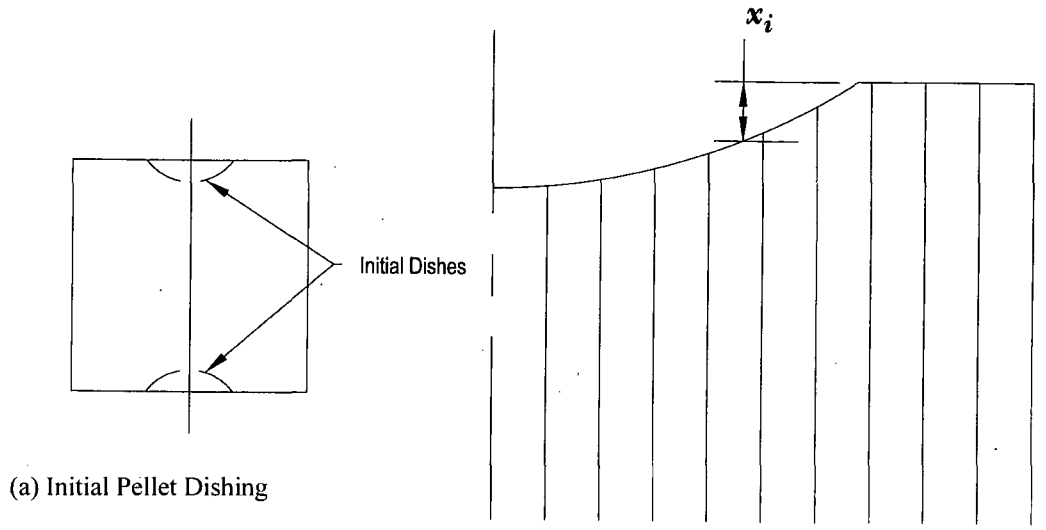

(a) Initial Pellet Dishing

(b) Dish Depth x_i for Ring i

Figure 7.10 Dished Pellet Geometry

References

[7-1] O.C. Zienkiewicz, "The Finite Element Method in Engineering Science," McGraw-Hill, 1971.
[7-2] J.S. Przenieniecki, "Theory of Matrix Structural Analysis," McGraw-Hill, 1968.

8. FISSION GAS RELEASE

As fuel is irradiated, fission products, including gaseous fission products, are generated in the fuel pellet. A fraction of the gaseous fission products is released to the fuel rod void volume. At any time during irradiation, the fraction of fission gas released is a function of both the temperature distribution in the fuel pellet and the exposure. The inventory of released fission gases consists primarily of xenon, krypton, and helium. In the PRIME code, the releases of xenon and krypton and the release of helium are addressed by separate models. The models are described below.

8.1 RELEASE OF (Xe + Kr)

The basic picture of the fission gas release (FGR) mechanism is summarized as follows:

[[

Global Nuclear Fuel

A Joint Venture of GE, Toshiba, & Hitachi

Global Nuclear Fuel
A Joint Venture of GE, Toshiba, & Hitachi

Global Nuclear Fuel

A Joint Venture of GE, Toshiba, & Hitachi

Global Nuclear Fuel

A Joint Venture of GE, Toshiba, & Hitachi

]]

[[

]]

Fig.8.1 Threshold temperature for grain boundary FP bubble interlinkage

[[

]]

Fig.8.2 Calculation method of effective time for time-dependent fission gas release.

Global Nuclear Fuel
A Joint Venture of GE, Toshiba, & Hitachi

[[

]]

8.2 HELIUM GENERATION AND RELEASE

[[

]]

The effects of helium generation and release are included through empirical correlation of helium release data. [[

]]

[[

]]

Figure 8.3 Predicted versus Measured Specific Helium Release

8.3 REFABRICATION OPTION

A recent advance in obtaining high exposure fuel performance data, particularly fuel centerline temperature data, is the refabrication and reirradiation of fuel rod test segments. In this process, fuel rod test segments are irradiated to a target exposure. The segment is then opened in a hot cell, a center hole is drilled in the pellet stack, a (new) thermocouple is inserted, the segment is refilled with a specific gas mixture, and the segment is then reinserted into the reactor and irradiated to higher exposure. This process eliminates the problems with thermocouple reliability and decalibration normally associated with high exposure temperature measurements using bimetallic thermocouples.

To permit simulation of such experiments, the PRIME code includes the capability to simulate the refabrication process. The step at which refabrication is to be simulated is flagged by the user and the details of the refill gas mixture (components and gram-moles of each component) are specified in the input. In the PRIME analysis, when the flagged step is reached, the calculated fuel rod internal gas mixture (including fill gas and released fission gases) is replaced by the refill gas mixture. The analysis then continues as normal.

References

[8-1] C. Vitanza et al., "Fission Gas Release from In-Pile Pressure Measurements", HPR-221.10 paper 38, presented at the EHPG Loen, 1978.
[8-2] J. A. Turnbull, "An Assessment of Fission Gas Release and the Effect of Microstructure at High Burn-up", HWR-604 (1999).
[8-3] M. Mogensen, J.H. Pearce and C.T. Walker, "Behaviour of Fission Gas in the Rim Region of High Burn-up UO_2 Fuel Pellets with Particular Reference to Results from an XRF Investigation", J. Nucl. Mater. 264 (1999) 99-112.
[8-4] R. Manzel et al, "HIGH BURNUP FUEL MICROSTRUCTURE AND ITS EFFECT ON FUEL ROD PERFORMANCE", ANS International Topical Meeting on Light Water Reactor Fuel Performance, Park City, October 2002.

9. ROD INTERNAL GAS PRESSURE

Assuming ideal communication between the fuel rod void volumes so that there are no pressure gradients, the fuel rod internal gas pressure is calculated from the ideal gas law as

$$P = \frac{\eta R}{\sum_i \left(\frac{V}{T}\right)_i} \tag{9-1}$$

where

P = fuel rod internal pressure (psia)

η = total amount of fill gas and fission gas occupying the fuel rod void volume (gm-moles)

R = universal gas constant = 40.872 in-lb_f/gm-mole-°R

$\left(\frac{V}{T}\right)_i$ = volume/temperature of fuel rod void volume i (in^3/°R)

The fuel rod void volume is assumed to consist of the fuel-cladding diametral gap, radial and transverse pellet cracks, pellet dishing, pellet center hole (hollow pellets), fuel rod plenum, and additional free volume resulting from pellet chamfers and fuel column loading (stacking) effects. [[

Global Nuclear Fuel

A Joint Venture of GE, Toshiba, & Hitachi

Global Nuclear Fuel
A Joint Venture of GE, Toshiba, & Hitachi

]]

APPENDIX A FINITE ELEMENT RELATIONS FOR MECHANICS SOLUTION

The PRIME model performs coupled thermal and mechanical analyses. The mechanical analysis utilizes a finite element based mechanics formulation. A summary of the finite element formulation and derivation of the element used in the PRIME model are presented below.

[[

]]

[[

]]

Figure A.1 Ring Element

[[

Global Nuclear Fuel

A Joint Venture of GE, Toshiba, & Hitachi

Global Nuclear Fuel
A Joint Venture of GE, Toshiba, & Hitachi

Global Nuclear Fuel

A Joint Venture of GE, Toshiba, & Hitachi

Global Nuclear Fuel
A Joint Venture of GE, Toshiba, & Hitachi

Global Nuclear Fuel

A Joint Venture of GE, Toshiba, & Hitachi

]]

[[

]]

Figure A.2 Limits for Volume and Area Integrations

[[

Global Nuclear Fuel

A Joint Venture of GE, Toshiba, & Hitachi

]]

[[

]]

Figure A.3 Sign Convention for Applied Pressure Increment Δp_1 and Δp_2

[[

Global Nuclear Fuel
A Joint Venture of GE, Toshiba, & Hitachi

]]

APPENDIX B DERIVATION OF (INCREMENTAL) MATERIAL COMPLIANCE MATRIX

Implementation of the finite element mechanics solution described in Appendix A requires that the material compliance matrix be stated in incremental form. Derivation of the material compliance matrix formulation used in the PRIME code is presented below.

[[

Global Nuclear Fuel

A Joint Venture of GE, Toshiba, & Hitachi

Global Nuclear Fuel

A Joint Venture of GE, Toshiba, & Hitachi

Global Nuclear Fuel

A Joint Venture of GE, Toshiba, & Hitachi

Global Nuclear Fuel

A Joint Venture of GE, Toshiba, & Hitachi

]]

[[

]]

Figure B.1 Definition of Tangent Modulus E_T and Generalized Strain Increments $\Delta\varepsilon^E$, $\Delta\varepsilon^P$, and $\Delta\varepsilon$

Global Nuclear Fuel
A Joint Venture of GE, Toshiba, & Hitachi

[[

Global Nuclear Fuel

A Joint Venture of GE, Toshiba, & Hitachi

Global Nuclear Fuel
A Joint Venture of GE, Toshiba, & Hitachi

Global Nuclear Fuel
A Joint Venture of GE, Toshiba, & Hitachi

]]

GNF

Global Nuclear Fuel

A Joint Venture of GE, Toshiba, & Hitachi

NEDO-33257
Class I
DRF 0000-0053-5423
January 2007

LICENSING TOPICAL REPORT

The PRIME Model for Analysis of Fuel Rod Thermal – Mechanical Performance Part 2 – Qualification

Disclaimer of Responsibility

This document was prepared by Global Nuclear Fuel (GNF). The use of this information for any purpose other than that for which it is intended is not authorized; and with respect to any unauthorized use, GNF makes no representation or warranty, expressed or implied, as to the completeness, accuracy or usefulness of the information contained in this document, or that its use may not infringe privately owned rights, and assumes no responsibility for liability or damage of any kind that may result from such use of this information.

Non-Proprietary Information Notice

This is a non-proprietary version of the document NEDC-33257P, which has the proprietary information removed. Portions of the document that have been removed are indicated by an open and closed bracket as shown here [[ ]].

TABLE OF CONTENTS

LIST OF FIGURES

SUMMARY

The PRIME model and computer program have been developed to provide best-estimate predictions of the thermal and mechanical performance of LWR nuclear fuel rods experiencing variable power histories. The PRIME code has been developed from the GESTR-Mechanical (GSTRM) code by (1) incorporating new models to address specific high exposure mechanisms identified and quantified since the original development of GSTRM and approval of GSTRM and its associated application methodology by the NRC in 1985[1-1], (2) modifying existing material properties relations to reflect current materials properties data, including the effects of exposure where appropriate, and (3) modifying existing submodels to reflect high exposure experimental data that has become available since the original development of GSTRM.

The PRIME code addresses the effects of fuel/cladding thermal expansion, fuel phase change volume change, fuel irradiation swelling, densification, relocation and fission gas release, fuel-cladding axial slip, cladding creepdown, irradiation hardening and thermal annealing of irradiation hardening, pellet and cladding plasticity and creep, pellet hot pressing and plastic collapse, and development of a porous pellet rim at high exposure.

PRIME performs coupled thermal and mechanical interaction analyses. The incremental finite element mechanics model performs an axisymmetric radial mechanical interaction analysis to determine pellet and cladding stresses and strains at the pellet midheight location. The thermal solution is obtained by numerical evaluation of the thermal conductivity integral. The mechanical and thermal calculations are coupled by a serial combination of the respective solutions.

This document is Part 2 of the PRIME Licensing Topical Report (LTR) and presents the experimental qualification of the PRIME model by comparison of integral code predictions of fuel rod temperatures, fuel rod fission gas release and internal pressure and cladding deformations to experimental data. The technical bases of the PRIME model, including (1) descriptions of the technical bases for the PRIME component models and material properties relations and (2) a description of the overall structure of the PRIME model and implementation of the component models is presented in Part 1 of this LTR (NEDO-33256). The methodology for application of the PRIME code for licensing and design analyses is presented in Part 3 of this LTR (NEDO-33258).

1. INTRODUCTION

The PRIME model and computer program has been developed to provide best-estimate predictions of the thermal and mechanical performance of LWR nuclear fuel rods experiencing variable power histories. The PRIME code has been developed from the GESTR-Mechanical (GSTRM) code by (1) incorporating new models to address specific high exposure mechanisms identified and quantified since the original development of GSTRM and approval of GSTRM and its associated application methodology by the NRC in 1985[1-1] [1-2], (2) modifying existing material properties relations to reflect current materials properties data, including the effects of exposure where appropriate, and (3) modifying existing submodels to reflect high exposure experimental data that has become available since the original development of GSTRM.

New models incorporated to address specific high exposure mechanisms include development of a porous pellet rim at high exposure. Also fuel pellet relocation and fission gas release models have been modified to reflect high exposure data. Existing materials properties models modified to reflect current materials properties data include the dependency of fuel thermal conductivity on gadolinia; materials properties modified to reflect the effects of high exposure include fuel thermal conductivity and (annealed) Zircaloy irradiation creep and growth.

The modifications and additions noted above extend the capability of the PRIME code to [[ ]]. The ultimate proof of an analytical model lies in its ability to adequately predict experimental data. This document is Part 2 of the PRIME Licensing Topical Report (LTR) and demonstrates the predictive capability of the PRIME model relative to fuel centerline temperature (Section 2), cladding diametral and axial strains (Section 3), fuel rod fission gas release (Section 4) and fuel rod internal pressure (Section 5) by comparison of integral code predictions of these parameters to experimental (measured) data. Additionally, comparisons of code predictions to experimental data are presented for helium release and pellet grain growth (Sections 6 and 7, respectively). As will be discussed, the PRIME experimental qualification data base has been greatly expanded relative to the GSTRM data base and includes a significant amount of high exposure data, including fuel temperature data, fuel rod fission gas release and internal pressure data, and cladding deformation data. The technical bases of the PRIME model, including (1) descriptions of the technical bases for the PRIME component models and material properties relations and (2) a description of the overall structure of the PRIME model and implementation of the component models, is presented in Part 1 of this LTR (NEDO-33256) and the methodology for application of the PRIME code for licensing and design analyses is presented in Part 3 of this LTR (NEDO-33258).

On the basis of the PRIME LTR, NRC approval is requested for application of the PRIME code for licensing of LWR fuel rods to a peak pellet exposure limit of [[ ]]. In subsequent sections of this report 'exposure' and 'burnup' will be used interchangeably unless noted otherwise.

References

[1-1] GESTR-LOCA – A Model for the Prediction of Fuel Rod Thermal Performance, NEDE-23785-1-PA (Vol.1), June 1984.

[1-2] Acceptance for Referencing of Licensing Topical Report NEDE-24011-P-A Amendment 7 to Revision 6, GE Standard Application for Reactor Fuel Letter, C.O. Thomas (NRC) to J. S. Charnley (GE), MFN –036-85, March 1, 1985.

2. *FUEL TEMPERATURE*

The in-reactor centerline temperature of a fuel rod can be inferred from a temperature indicator, such as the measured radius of a fuel microstructural change (i.e., fuel melting, onset of columnar or equiaxed grain growth) to which a temperature can be assigned, or measured directly by insertion of a thermocouple in the fuel column. Although the fuel melting temperature is known with adequate certainty, this type of data is limited in application, as it can be obtained only from high-power operation, generally beyond the expected operating powers and temperatures for commercial fuel rods. The same problem exists, to a lesser extent, with temperature data inferred from the onset of columnar and equiaxed grain growth, with the added complexity of large uncertainties in assigning a grain growth temperature and irradiation time when the grain growth radius was set. Therefore, to minimize the variability in the experimental data, and to employ data over the entire power range of interest, the thermal qualification is performed by comparison to data obtained by direct in-reactor measurement of fuel temperatures by thermocouple or expansion thermometer. The experimental data is summarized in Section 2.1. More specific information is provided in Appendix A. Comparisons of predicted and measured temperatures are presented in Section 2.2.

2.1 Measured Data

GSTRM Qualification Data

IFA-21 – IFA-21 was irradiated in the Halden Boiling Heavy Water Reactor (HBWR) in the period from April 1965 to November 1966. The Zircaloy-2 (Zr-2) clad UO_2 fuel pellets were of 0.490 to 0.494 inch nominal outside diameter and 0.047 inch inside diameter for the insertion of the thermocouple. Pellet-cladding diametral gaps were nominally 2 and 6.5 mils. Nominal fuel densities were 96 and 98% of theoretical with a nominal enrichment of 5 wt% U-235. The pellets were spherically dished ~1.5 vol%. Active fuel column lengths were ~70 inches with the thermocouple located at approximately mid-height. Fuel center temperatures were measured during a ramp (~4 to 13 kW/ft) early in life (215 MWd/MTU) and during two ramps (~2 to 10 kW/ft) later in life (4300 MWd/MTU). Power operation between the ramps was erratic, varying from 5 to 14 kW/ft.

IFA-116 and IFA-117 – Two similar instrumented fuel assemblies, IFA-116 and IFA-117, were irradiated in the HBWR during 1968 – 1969. The zircaloy-2 clad UO_2 fuel pellets were 0.545 inch nominal outside diameter and 0.126 inch nominal inside diameter for the insertion of the thermocouple. One fuel rod contained all hollow pellets. Fabricated pellet-cladding diametral gaps varied from ~8 to 8.5 mils. Pellet densities were ~91.5 and 97% of theoretical with a nominal enrichment of 6 wt% U-235. All pellets had truncated cone dishes of ~2.2 vol%. Active fuel column lengths were ~20 inches with the thermocouple located in either the top or bottom 20% of the fuel column. Fuel center temperatures were measured during constant power operation (12 to 22 kW/ft) and occasional power ramps (1 to 21 kW/ft) throughout the irradiation.

IFA-410 – This instrumented fuel assembly was irradiated in the HBWR and contained two fuel rods equipped with central fuel thermocouples. The UO_2 fuel pellets varied in diameter from 0.477 to 0.481 inch to provide pellet cladding diametral gaps of either 7.9 or 11.8 mils. Pellet densities were 95% TD with a nominal enrichment of 7.1 wt% U-235. The fuel column length was 18.7 inches with the thermocouple located ~5 inches from the bottom of the fuel column. The fuel rods were filled with helium at 1 atmosphere. Fuel temperature measurements were taken during steady-state operation at power levels ranging from 9 to 13 kW/ft to rod average exposures of ~17,000 MWd/MTU.

IFA-411 - The IFA-411 assembly irradiated in the HBWR included on-line fuel centerline temperature measurements by thermocouple for one fuel rod. The UO_2 fuel pellets were of 95% TD, 7.1 wt% U-235 enrichment and 0.418 inch in diameter. The Zr-2 cladding outer diameter was 0.493 inch, with a thickness of 0.034 inch, resulting in a 7.0 mil pellet-cladding diametral gap. The fuel column length was 58.4 inches with the thermocouple located in the bottom ~10% of the fuel column. The helium pre-pressurization was 1 atmosphere. Fuel temperature measurements were taken during steady-state operation at power levels ranging from ~9 to 12 kW/ft to rod average exposures of ~30,000 MWd/MTU.

IFA-429 – This test assembly was sponsored by the United States Nuclear Regulatory Commission (USNRC) and was tested in the HBWR. The fuel rods were representative of PWR fuel design with ~26 atmospheres helium pre-pressurization. Two of the fuel rods were instrumented with thermocouples. Both of these fuel rods had an initial gap of 8.2 mils and the pellet densities were 91 and 93% TD, respectively. The fuel column length was 9.6 inches with the thermocouple located ~mid-height of the fuel stack. Temperature measurements were taken during steady-state operation at power levels ranging from 1 to 9.7 kW/ft to rod average exposures of ~13,000 and ~22,000 MWd/MTU.

[[

]]

IFA-431 and IFA-432 – This test was sponsored by the USNRC and was conducted in the HBWR. The two assemblies each contain six fuel rods operated at a peak power of about 15 kW/ft. The test fuel rod matrix included pellet-cladding diametral gaps of 3, 9, and 15 mils, pellet densities of 92 to 97% TD and helium or xenon fill gas. Temperature measurements were taken during steady-state operation at power levels from ~4 to 15 kW/ft, and rod average exposures up to ~22,000 MWd/MTU.

Global Nuclear Fuel
A Joint Venture of GE, Toshiba, & Hitachi

[[

]]

Additional Qualification Data

[[

]]

IFA-562 – The IFA-562 rig consisted of six fuel rods with expansion thermometers in four rods. The nominal pellet outer diameter was 0.233 inch, and the pellet-cladding diametral gap was 4 mil. The expansion thermometer was inserted through the whole length of the fuel column, which was ~17 inches in length. The pellet density was 94% TD with an enrichment of 13 wt% U-235. Temperature measurements were taken during steady-state operation at powers of 6 to 12 kW/ft to a rod average exposure of ~57,000 MWd/MTU.

The 3rd Riso Fission Gas Project (RISO-3) – This project was organized as a joint international project and executed by Riso during 1986-1990. A total of 15 bump tests were performed in the DR3 reactor at Riso. Ten fuel rods with thermocouples were selected for model comparison: five GE fuel rods of 8x8 type base-irradiated in commercial BWRs up to ~42,000 MWd/MTU, three ANF(Advanced Nuclear Fuels) fuel rods base-irradiated in commercial PWRs up to 15,000 - 44,000 MWd/MTU, and two Riso fuel rods base-irradiated in the Halden reactor up to 44,000 - 48,000 MWd/MTU. The rods after base-irradiation were cut for refabrication into short test fuels. The column length of the test fuel was about 10-12 inches with the thermocouple located ~2 inches from the top of the fuel column. Temperature measurements were taken during the bump tests at maximum power levels of 9.5 to 13.5 kW/ft at the thermocouples.

[[

]]

[1] An expansion thermometer utilizes the thermal expansion of a metal rod witch is located at the pellet centerline and extends along the full length of the fuel column. Expansion thermometers eliminate component of uncertainty arising from transmutation-induced decalibration of conventional high temperature at high burnup.

2.2 Comparisons of Predicted and Measured Temperatures

An overall comparison of predicted and measured fuel centerline temperature is presented in Figure 2-1. The ratios of predicted/measured fuel centerline temperature as a function of exposure are presented in Figure 2-2. In these figures, measured temperatures obtained from bi-metallic thermocouples have been corrected for in-reactor thermocouple decalibration.

[[

]]

Figure 2.1 Predicted versus Measured Fuel Temperature

[[

]]

Figure 2.2 Predicted/Measured Fuel Temperature versus Exposure

3. CLADDING DEFORMATION

Cladding deformations (strains) consist of elastic, thermal and permanent (plastic plus creep and irradiation growth) components. The cladding diametral and axial thermal strains can be accurately calculated as a function of temperature. The diametral and axial permanent strains are typically determined by comparing pre- and post-irradiation measurents of cladding diameter and length and adjusting for temperature differences (if any) in the measurement conditions. If pre-irradiation characterizations of diameter and length are not available, nominal tubing fabrication specifications can be used, although this introduces uncertainty in addition to that inherent in the various measurement techniques. Alternatively, a better approximation of the as-fabricated cladding diameter is provided by the measured cladding diameter in the fission gas plenum region of the rod. Additionally, measurements at different exposures may be used to infer incremental changes without introducing the uncertainty associated with lack of pre-irradiation characterizations. In some cases, cladding diametral and axial strains are measured during operation in instrumented test assemblies in test reactors such as Halden. These measurements yield total strains and can be used to compare predicted and measured elastic strains provided the measurements are adjusted for the other strain components. Measurements performed at different power levels or may be used to infer the impact of incremental power changes on cladding strain response. Data from all the measurement types above are used for the cladding deformation qualification. The experimental data is summarized in Section 3.1. More specific information is provided in Appendix A. Comparisons of predicted and measured temperatures are presented in Section 3.2.

3.1 Measured Data

GSTRM Qualification Data

[[

]]

Inter Ramp Test Rods – Twenty fuel rods, representative of 8x8 BWR fuel designs, were base irradiated at power levels ranging from 7 to 14 kW/ft to exposures of either ~10,000 MWd/MTU or ~20,000 MWd/MTU. Subsequent to the base irradiation, the fuel rods were power ramped to peak powers ranging from ~12 to 20 kW/ft. These variables included cladding heat treatment, pellet-cladding diametral gap, and pellet density. Cladding diameter and length measurements were made before and after the final power ramp. Comparisons of the predicted and measured cladding diameter and length change during the power ramp are presented in Figures 3-1 through 3-4.

Super Ramp Test Rods – These six fuel rods are also part of the qualification database for the fission gas release model. They were base irradiated at low-to-moderate power levels in commercial reactors to rod average exposures of ~35,000 MWd/MTU. Subsequent to the base irradiation, the fuel rods were inserted in the R2 reactor in Studsvik, Sweden and power ramped to peak powers ranging from ~10 to 15 kW/ft. Cladding diameter measurements were made on all six fuel rods before and after the base irradiation and after the power ramp. Comparisons of the predicted and measured cladding diameter change both during the base irradiation and during the power ramp are presented in Figures 3-1 and 3-2.

Development Test Rods – These fuel rods are also part of the calibration and qualification data bases for the fission gas release model. Test variables included cladding thickness and pellet density. These fuel rods were base irradiated at power levels of 15 to 23 kW/ft with exposures up to 70,000 MWd/MTU. Figures 3-1 and 3-2 compare the predicted and measured permanent cladding diameter change, and Figures 3-3 and 3-4 compare the predicted and measured cladding permanent length change.

BR-3 High Burnup Fuel Rods – These five fuel rods are also part of the qualification database for the fission gas release model. The fuel rods were base irradiated in the BR-3 PWR in Mol, Belgium at peak powers from ~13 to 18 kW/ft to rod average exposures of 49,000 to 62,000 MWd/MTU as part of the United States Department of Energy (USDOE) sponsored BR-3 High Burnup Program. Figures 3-1 and 3-2 compare the predicted and measured permanent cladding diameter change, for several axial positions, and Figures 3-3 and 3-4 compare the predicted and measured cladding permanent length change.

[[

]]

Additional Qualification Data

[[

]]

Global Nuclear Fuel
A Joint Venture of GE, Toshiba, & Hitachi

]]

3.2 Comparisons of Predicted and Measured Cladding Deformations

Comparisons of predicted and measured cladding deformations are presented in Figures 3-1 through 3-4. An overall comparison of predicted and measured cladding permanent diametral strains (%ΔD/D) is presented in Figure 3-1. The figure includes data from measurements of cladding creepdown during long-term base irradiation as well as outward cladding deformation due to pellet-cladding interaction during high power steady-state operation and rapid power ramps. The differences between predicted and measured cladding diametral strains for the same data as a function of rod average exposure is presented in Figure 3-2. An overall comparison of predicted and measured cladding permanent axial strains (%ΔL/L) is presented in Figure 3-3. The differences between predicted and measured cladding axial strains for the same data as a function of rod average exposure is presented in Figure 3-4.

[[

]]

Figure 3.1 Predicted versus Measured Permanent Cladding Diametral Strain

[[

]]

Figure 3.2 Predicted Minus Measured Permanent Cladding Diametral Strain versus Exposure

[[

]]

Figure 3.3 Predicted versus Measured Permanent Cladding Axial Strain

[[

]]

Figure 3.4 Predicted Minus Measured Permanent Cladding Axial Strain versus Exposure

4. FISSION GAS RELEASE

A significant fraction of the experimental data to which the fission gas release model was calibrated was obtained from irradiation capsules that were short and/or experienced relatively constant power operation with relatively flat axial power distributions. The intent of this section is to demonstrate the fission gas release model predictive capability for longer fuel rods that have experienced either widely varying operating histories or highly peaked and time-varying axial power distributions.

The single most important prerequisite of experimental data considered for use in qualification of the fission gas release prediction capability is that the power-exposure history be well-characterized. This prerequisite exists because of the high sensitivity of the fission gas release model to fuel temperature and exposure. Therefore, of the fission gas release data currently available, the qualification database has been selected on the basis of availability of well-characterized power histories. Additionally, GNF has historically used only fission gas data obtained by fuel rod puncturing for model calibration and qualification. However, GNF has recently verified the accuracy of fission gas measured performed by in-pool plenum gamma scanning and is now using fission gas data obtained by this technique, in addition to puncture data, for model calibration and qualification.

The experimental data is summarized in Section 4.1. More specific information is provided in Appendix A. Comparisons of predicted and measured temperatures are presented in Section 4.2.

4.1 Measured Data

GSTRM Qualification Data

For qualification of the GSTRM model, GNF assembled an experimental database for fission gas release that included fuel rod puncture and gas collection measurements from approximately [[ ]] fuel rods for which detailed operating power histories were available. This database included:

a. [[

]]

b. Development Fuel Rods – Fission gas release measurements have been obtained from a number of developmental programs where fuel has been operated in test reactors or base irradiated in commercial reactors and later moved to a test reactor for further irradiation. Such fuel rods represent a wide variety of fuel designs and have been operated over a wide range of powers (up to 48 kW/ft) and exposures (up to 99,000 MWd/MTU). Portions of this database were obtained from industry group sponsored programs such as the Battelle High Burnup Effects Program, OECD Halden Reactor Project, RISO High Burnup Fission Gas Release Program, and the Inter-Ramp, Over-Ramp, Super-Ramp, and GAIN industry-sponsored Programs.

Additional Qualification Data

[[

]]

Development Rods

High Burnup Effects Program-2 (HBEP-2) and HBEP-3, fission gas release data for 15 rods with rod average exposures up to ~49000 MWd/MTU (HBEP-2) and 27 rods with rod average exposures up to ~70000 MWd/MTU (HBEP-3) was obtained by puncturing and gas collection. Some of these rods are rods for which cladding profilometry was performed as described in Section 3.1.

In a GE program, 8x8 rods containing aluminosilicate additives were irradiated in instrumented fuel assemblies in the Halden reactor under a bilateral agreement between GE and OECD HRP to determine the effects of aluminosilicate additives on fuel fission gas release. Fission gas measurements

for 4 rods were performed by puncturing and gas collection after operation up to ~49000 MWd/MTU. These are the same assemblies for which fuel temperature measurements were performed as described in Section 2.1.

4.2 Comparisons of Predicted and Measured Fission Gas Release

Comparisons of predicted and measured fission gas release are presented in Figures 4-1 through 4-3. An overall comparison of predicted and measured fission gas release is presented in Figure 4-1. The differences between predicted and measured fission gas releases as a function of rod average exposure for cases in which the measured release is less than 5% is presented in Figure 4-2. The ratios of predicted/measured fission gas release as a function for rod average exposure for cases in which the measured release is greater than 5% is presented in Figure 4-3.

[[

]]

Figure 4.1 Predicted versus Measured Fission Gas Release

[[

]]

Figure 4.2 Predicted minus Measured Fission Gas Release versus Exposure

[[

]]

Figure 4.3 Predicted/Measured Fission Gas Release versus Exposure

5. FUEL ROD INTERNAL PRESSURE

The fuel rod internal pressure is determined by (1) the as-fabricated fuel rod characteristics such as the as-fabricated void volume and fill gas pressure, (2) the release of gaseous fission products from the fuel pellets to the fuel rod void volume, (3) changes in the fuel rod geometry during irradiation, and (4) the temperature of the gas occupying the fuel rod void volume. The as-fabricated fuel rod characteristics are known from the specified fabrication tolerances or available pre-characterization. The fission gas release prediction capability is demonstrated in Section 4 for fuel rod exposure up to ~100,000 MWd/MTU. The predicted changes in the fuel rod geometry are based upon separate effects measurements of the fuel and cladding dilation mechanisms and the integral fuel rod deformation prediction capability is demonstrated in Section 3 for fuel rod exposures up to 83,000 MWd/MTU. The purpose of the experimental qualification presented in this section is primarily to address the remaining item regarding the effect of gas temperature due to fuel rod heat-up on rod internal pressure. This pressure is also of significane relative to related analyses of LOCA and dry storage of spent fuel.

The fuel rod void volume is comprised of the fuel-cladding diametral gap, radial and transverse pellet cracks, pellet dishes, pellet center hole (hollow pellets), fuel rod plenum, and additional free volume due to pellet chamfers and fuel column loading (stacking) effects. The PRIME fuel rod internal pressure calculation distributes the gas inventory to these various void volumes and assigns an appropriate temperature to the gas in each void volume. For example, the gap average temperature is assigned to the gas in the pellet-cladding diametral gap, the adjacent fuel temperature is assigned to the gas occupying pellet crack volumes. Figure 5-3 confirms the ability of the PRIME model to reliably predict hot operating fuel rod internal pressure.

The experimental data is summarized in Section 5.1. More specific information is provided in Appendix A. Comparisons of predicted and measured temperatures are presented in Section 5.2.

5.1 Measured Data

GSTRM Qualification Data

IFA-116 and IFA-117 – Six of the fuel rods in assemblies IFA-116 and IFA-117 were continuously monitored for internal pressure via in-reactor fuel rod pressure transducers. Fuel rod average powers varied from 10.6 to 22.5 kW/ft to exposures of 9000 MWd/MTU.

IFA-429 – Nine fuel rods in the assembly were instrumented for fuel rod internal pressure measurements. Three of the fuel rods were selected as typical and modeled. Rod average powers range between 4.5 and 10.5 kW/ft to exposures of 20,500 MWd/MTU.

[[

]]

Global Nuclear Fuel
A Joint Venture of GE, Toshiba, & Hitachi

Additional Qualification Data

IFA-562 – The IFA-562 rig consisted of six fuel rods and two of them were equipped with pressure sensors. The nominal pellet outer diameter was 0.233 inch, and the pellet-cladding diametral gap was 4 mil. The pellet density was 94% TD with an enrichment of 13 wt% U-235. Initial helium fill gas pressure was 10 atmosphere. Pressure measurements were taken during steady-state operation at powers of ~6 to 13 kW/ft to a rod average exposure of ~58,000 MWd/MTU.

RISO3 - This project was organized as a joint international project and executed by the RISO national laboratory during 1986-1990. A total of 15 bump tests were performed in the DR3 reactor at RISO. Ten fuel rods with pressure transducers were selected for model comparison: five GE fuel rods of 8x8 type base-irradiated in commercial BWRs up to ~42,000 MWd/MTU, four ANF(Advanced Nuclear Fuels) fuel rods base-irradiated in commercial PWRs up to ~44,000 MWd/MTU, and one Riso fuel rod base-irradiated in the Halden reactor up to ~48,000 MWd/MTU. The rods after base-irradiation were cut for refabrication into short test rods. Internal pressure measurements were taken during the bump tests at maximum power level of ~10.5 to 13.8 kW/ft.

5.2 Comparisons of Predicted and Measured Rod Internal Pressure

Comparisons of predicted and measured rod internal pressure are presented in Figures 5-1 and 5-2. An overall comparison of predicted and measured rod internal pressure is presented in Figure 5-1. The differences between predicted and measured rod internal pressure as a function of rod average exposure is presented in Figure 5-2.

[[

]]

Figure 5.1 Predicted versus Measured Fuel Rod Internal Pressure

[[

]]

Figure 5.2 Predicted Minus Measured Fuel Rod Internal Pressure versus Exposure

6. HELIUM RELEASE

[[

]]

6.1 Measured Data

GSTRM Qualification Data

[[

]]

Global Nuclear Fuel
A Joint Venture of GE, Toshiba, & Hitachi

Additional Qualification Data

[[

]]

6.2 Comparisons of Predicted and Measured Helium Release

Comparisons of predicted and measured helium gas release are presented in Figures 6-1 and 6-2. An overall comparison of predicted and measured helium release is presented in Figure 6-1. The ratios of predicted/measured helium release as a function for rod average exposure is presented in Figure 6-2. In Figures 6-1 and 6-2, the predicted and measured helium amounts are total helium amounts and include both initial helium fill gas and released helium.

[[

]]

Figure 6.1 Predicted versus Measured Fuel Rod Total Helium Release

[[

]]

Figure 6.2 Predicted/Measured Fuel Rod Total Helium Release versus Exposure

7. PELLET GRAIN GROWTH

The PRIME fission gas release model includes a grain size dependency. Thus the PRIME model also includes a grain growth model. The grain growth model includes a direct temperature dependency and an indirect exposure dependency through the dependency on fractional coverage of grain boundaries by fission gas bubbles.

The measured grain size data used in qualification of the grain growth model is based upon metallography of unirradiated and irradiated fuel pellets. Because of the sensitivity of grain growth to both temperature and exposure, only metallography from rods with well-characterized power histories are used in the qualification.

The experimental data is summarized in Section 7.1. More specific information is provided in Appendix A. Comparisons of predicted and measured temperatures are presented in Section 7.2.

7.1 Measured Data

GSTRM Qualification Data

Not applicable.

Global Nuclear Fuel
A Joint Venture of GE, Toshiba, & Hitachi

Additional Qualification Data

[[

]]

7.2 Comparisons of Predicted and Measured Grain Size

Comparisons of predicted and measured grain size are presented in Figures 7-1 and 7-2. An overall comparison of predicted and measured grain size is presented in Figure 7-1. The ratios of predicted/measured grain size as a function of rod average exposure is presented in Figure 7-2.

[[

]]

Figure 7.1 Predicted vs Measured Grain Size

[[

]]

Figure 7.2 Predicted/Measured Grain Size versus Exposure

APPENDIX A DETAILED DESCRIPTION OF EXPERIMENTAL DATA BASES

A.1 Fuel Centerline Temperatures

GSTRM Qualification Data

Identification	Comments	# of Rods	Exposure at Thermocouple GWD/Mtu
HRP_IFA21		3	5.0
HRP_IFA116		1	4.5
HRP_IFA117		3	9.5
HRP_IFA410		2	14.2
HRP_IFA411		1	31.3
[[			]]
HRP_IFA429		2	22.4
HRP_IFA431		4	5.5
HRP_IFA432		5	35.4
[[			
			]]

Additional Qualification Data

Identification	**Comments**	**# of Rods**	**Exposure at Thermocouple GWD/Mtu**
[[			]]
HRP_IFA562	small diameter; Halden test reactor; expansion thermometer	4	57.4*
RISO3	5 GE rods: 8x8 BWR; base irradiated in commercial BWRs 3 ANF rods: base irradiated in a commercial PWR 2 Riso rods: base irradiated in Halden test reactor All rods: ramp tested in DR3 test reactor	10	50.1
[[			]]

A.2.1 Cladding Diametral Deformations

GSTRM Qualification Data

Identification	Comments	# of Rods	Rod Average Exposure GWD/Mtu
[[			
			]]

Additional Qualification Data

Identification	Comments	# of Rods	Rod Average Exposure GWD/Mtu
[[			
			]]

A.2.2 Cladding Axial Deformations

GSTRM Qualification Data

Identification	Comments	# of Rods	Rod Average Exposure GWD/Mtu
[[			
			]]

Additional Qualification Data

Identification	Comments	# of Rods	Rod Average Exposure GWD/Mtu
[[			
			]]

A.3 Fission Gas Release

GSTRM Qualification Data

Identification	Comments	# of Rods	Rod Average Exposure GWD/Mtu
[[			
			]]

Global Nuclear Fuel
A Joint Venture of GE, Toshiba, & Hitachi

GSTRM Qualification Data (continued)

Identification	Comments	# of Rods	Rod Average Exposure GWD/Mtu
[[			
			]]

Global Nuclear Fuel
A Joint Venture of GE, Toshiba, & Hitachi

Additional Qualification Data

Identification	Comments	# of Rods	Rod Average Exposure GWD/Mtu
[[			
			]]

A.4 Rod Internal Pressure

GSTRM Qualification Data

Identification	Comments	# of Rods	Rod Average Exposure GWD/Mtu
HRP_IFA116		2	4.6
HRP_IFA117		4	9.0
HRP_IFA429		3	20.5
[[			]]

Global Nuclear Fuel
A Joint Venture of GE, Toshiba, & Hitachi

Additional Qualification Data

Identification	**Comments**	**# of Rods**	**Rod Average Exposure GWD/Mtu**
HRP_IFA562	small diameter; Halden test reactor	2	58.1
RISO3	5 GE rods: 8x8 BWR; base irradiated in commercial BWRs 4 ANF rods: base irradiated in a commercial PWR 1 Riso rod: base irradiated in Halden test reactor All rods: ramp tested in DR3 test reactor	10	48.6

A.5 Helium Gas Release

GSTRM Qualification Data

Identification	Comments	# of Rods	Rod Average Exposure GWD/Mtu
[[			
			]]

Additional Qualification Data

Identification	Comments	# of Rods	Rod Average Exposure GWD/Mtu
[[			
			]]

A.6 Pellet Grain Growth

GSTRM Qualification Data – Not Applicable

Additional Qualification Data

Identification	Comments	# of Rods	Rod Average Exposure GWD/Mtu
[[			
			]]

Global Nuclear Fuel

A Joint Venture of GE, Toshiba, & Hitachi

NEDO-33258
Class I
DRF 0000-0053-5423
January 2007

LICENSING TOPICAL REPORT

The PRIME Model for Analysis of Fuel Rod Thermal – Mechanical Performance Part 3 – Application Methodology

Global Nuclear Fuel
A Joint Venture of GE, Toshiba, & Hitachi

Disclaimer of Responsibility

This document was prepared by Global Nuclear Fuel (GNF). The use of this information for any purpose other than that for which it is intended is not authorized; and with respect to any unauthorized use, GNF makes no representation or warranty, expressed or implied, as to the completeness, accuracy or usefulness of the information contained in this document, or that its use may not infringe privately owned rights, and assumes no responsibility for liability or damage of any kind that may result from such use of this information.

Non-Proprietary Information Notice

This is a non-proprietary version of the document NEDO-33258, which has the proprietary information removed. Portions of the document that have been removed are indicated by an open and closed bracket as shown here [[ ]].

TABLE OF CONTENTS

LIST OF FIGURES

TABLES

SUMMARY

The PRIME model and computer program has been developed to provide best-estimate predictions of the thermal and mechanical performance of LWR nuclear fuel rods experiencing variable power histories. The PRIME code has been developed from the GESTR-Mechanical (GSTRM) code by (1) incorporating new models to address specific high exposure mechanisms identified and quantified since the original development of GSTRM and approval of GSTRM and its associated application methodology by the NRC in 1985 (Reference 8), (2) modifying existing material properties relations to reflect current materials properties data, including the effects of exposure where appropriate, and (3) modifying existing submodels to reflect high exposure experimental data that has become available since the original development of GSTRM.

The PRIME code addresses the effects of fuel/cladding thermal expansion, fuel phase change, volume change, fuel irradiation swelling, densification, relocation and fission gas release, fuel-cladding axial slip, cladding creepdown, irradiation hardening and thermal annealing of irradiation hardening, pellet and cladding plasticity and creep, pellet hot pressing and plastic collapse, and development of a porous pellet rim at high exposure.

PRIME performs coupled thermal and mechanical interaction analyses. The incremental finite element mechanics model performs an axisymmetric radial mechanical interaction analysis to determine pellet and cladding stresses and strains at the pellet midheight location. The thermal solution is obtained by numerical evaluation of the thermal conductivity integral.

This document is Part 3 of the PRIME Licensing Topical Report and presents a description of the methodology for application of the PRIME code for licensing and design applications. The technical bases of the PRIME model, including (1) descriptions of the technical bases for the PRIME component models and material properties relations and (2) a description of the overall structure of the PRIME model and implementation of the component models is presented in Part 1 of this LTR (NEDO-33256) and the experimental qualification of the PRIME model by comparison of integral code predictions of fuel rod temperatures, fuel rod fission gas release and internal pressure, and fuel rod strain to experimental data is presented in Part 2 of this LTR (NEDO-33257).

1. INTRODUCTION

The PRIME model and computer program has been developed to provide best-estimate predictions of the thermal and mechanical performance of $(U,Gd)O_2$ LWR nuclear fuel rods experiencing variable power histories. The PRIME code has been developed from the GESTR-Mechanical (GSTRM) code by (1) incorporating new models to address specific high exposure mechanisms identified and quantified since the original development of GSTRM and approval of GSTRM and its associated application methodology by the NRC in 1985 (References 8, 9), (2) modifying existing material properties relations to reflect current materials properties data, including the effects of exposure where appropriate, and (3) modifying existing submodels to reflect high exposure experimental data that has become available since the original development of GSTRM.

New models incorporated to address specific high exposure mechanisms include development of a porous pellet rim at high exposure. Existing materials properties models modified to reflect current materials properties data include the dependency of fuel thermal conductivity on gadolinia; materials properties modified to reflect the effects of high exposure include fuel thermal conductivity and (annealed) Zircaloy irradiation creep and growth. Existing submodels modified to reflect high exposure data include the pellet relocation model and the pellet fission gas release model.

The modifications and additions noted above were intended to extend the capability of the PRIME code to [[ ]], so that it can be utilized to license new high exposure fuel designs. This document is Part 3 of the PRIME Licensing Topical Report (LTR) and describes the application methodology by which the PRIME model will be utilized to specify Linear Heat Generation Rate (LHGR) versus (peak pellet) exposure operating limits for any axial location in a fuel rod, and the overpower limits related to those LHGR limits, such that operation within these limits assures compliance with all fuel rod thermal mechanical design and licensing criteria. These limits will be utilized during core design and plant monitoring to ensure that operation of the fuel rod is maintained within analyzed bases. The technical bases of the PRIME model, including (1) descriptions of the technical bases for the PRIME component models and material properties relations and (2) a description of the overall structure of the PRIME model and implementation of the component models, is presented in Part 1 of this LTR (NEDO-33256) and the experimental qualifications of the PRIME model by comparison of integral code predictions of fuel rod temperatures, fuel rod fission gas release, internal pressure and cladding deformations to experimental data is presented in Part 2 of this LTR (NEDO-33257).

On the basis of the PRIME LTR, NRC approval is requested for application of the PRIME code for licensing of LWR fuel rods to a peak pellet exposure limit of [[ ]] GWd/MTU. In subsequent sections of this report 'exposure' and 'burnup' will be used interchangeably unless noted otherwise.

1.1. BACKGROUND

The fuel rod cladding surrounding the uranium dioxide fuel pellets represents the primary barrier to the release of radioactive fission products to the reactor coolant. Although the nuclear power plant system is designed to accommodate a level of activity release that may result from defective fuel rods, the Global Nuclear Fuel (GNF) fuel rod design objective is to preclude systematic defects from arising under the condition of licensed operation including normal steady-state operation and anticipated operational occurrences. In particular, GE/GNF has established a process, documented in GESTAR (Reference 1), to ensure that fuel rod mechanical integrity and safe operation is maintained throughout the fuel rod design lifetime. The design criteria included in the process were developed by GE/GNF and other specific industry groups to focus on the parameters that are most significant to fuel performance and operating occurrences that can realistically limit fuel performance and impact safe operation. The specific criteria are patterned after ANSI/ANS 57.5-1981 (Reference 5) and NUREG-0800 Rev. 2 (Reference 6).

As stated above, GNF presently licenses fuel utilizing the GESTR-Mechanical model (Reference 4), and as accepted by the NRC staff (Reference 8), to ensure that design requirements (Reference 1 Section 1.1.2A and 1.1.2B i, vi, ix, and x) are maintained. GNF plans to utilize the currently approved GESTR-Mechanical application methodology with the new PRIME model (Engineering Computer Program- ECP). This includes the statistical propagation of errors for [[
]] The basic methods, including model uncertainties associated with the application of the PRIME model, are discussed below in Section 1.3. The analysis inputs and procedures for each type of analysis are covered in Section 3.4 of this document.

1.2. SUMMARY OF METHODOLOGY

To achieve design objectives with confidence, while utilizing the full mechanical capabilities of the fuel rod design, a thorough design analysis methodology has been developed by Global Nuclear Fuel. This analysis methodology is comprised of three elements:

1. Design criteria - Mechanistic design criteria (Design Limits) are applied to those parameters that realistically represent fuel performance limitations (See Section 2),

2. Analytical model - An improved fuel behavior analytical model has been developed (See Reference 2). The PRIME fuel behavior model has been developed as a best estimate predictor to enable an accurate estimate of the expected fuel performance while also enabling realistic assessment of design parameter sensitivities. PRIME has been qualified to extensive experimental fuel performance measurements to enable clear quantification of the fuel performance prediction uncertainty (See Reference 3), and

3. Statistical/Worst Tolerance analysis procedure - Statistical or worst tolerance methodology, in conjunction with the best estimate PRIME fuel performance predictor, enables a realistic assessment of the individual and combined design parameter sensitivities. Statistical analysis methodology permits direct application of the fuel rod design parameter and operation uncertainties to provide a quantitative assessment of the design analysis conservatism considering the range of applications. The worst tolerance methodology allows a conservative quantification of a worst tolerance application.

1.3. OVERVIEW OF STATISTICAL AND WORST TOLERANCE ANALYSES

GNF utilizes both statistical and worst tolerance analyses to adequately ensure that the licensed operation for a fuel rod design meets all fuel rod thermal-mechanical design requirements as covered in Reference 1.

1.3.1. Statistical Analyses

The thermal analysis, fuel rod internal pressure analysis, overpower to incipient fuel centerline melting analysis, and cladding mechanical analysis are performed statistically by applying the standard error propagation equation to the results of a PRIME best estimate (nominal) case and multiple single parameter perturbation analyses, as follows:

$$[[\sigma_P^2 = \sum_{i=1}^{n}\left[\frac{\partial P}{\partial x_i}\right]^2 \sigma_{x_i}^2 + 2\sum_{i=1}^{n-1}\sum_{j=i+1}^{n}\frac{\partial P}{\partial x_i}\frac{\partial P}{\partial x_j}\sigma_{x_i}\sigma_{x_j}\rho_{x_i,\,x_j}$$

where:

σ_P	=	Standard deviation of the PRIME output parameter being analyzed (internal pressure, local plastic strain, etc.).
i,j	=	Index for input variables which are perturbed in the error propagation analysis.
n	=	Total number of input variables x_i, x_j which are perturbed in the error propagation analysis.
x_i, x_j	=	Input variable perturbed in the PRIME analysis.

$\frac{\partial P}{\partial x_i}, \frac{\partial P}{\partial x_j}$ = Partial derivative of PRIME output parameter P with respect to perturbed PRIME input variable x_i, x_j.

$\sigma_{x_i}, \sigma_{x_j}$ = Standard deviation of the perturbed PRIME input variable.

ρ_{x_i, x_j} = Correlation coefficient for variables x_i, x_j.

The evaluation of output parameter variances using the error propagation equation is performed as follows. A PRIME analysis is performed with all inputs at their best estimate values. This analysis establishes the best estimate (nominal) value of the output parameter P_{nom}. Additional PRIME analyses are then performed with each input variable (x_i) individually perturbed two standard deviations (with some exceptions) from its best estimate value in the direction that worsens the output parameter being analyzed. The results from these perturbation analyses are then utilized with the best estimate results to calculate finite difference approximations of the partial derivatives as follows for use in the error propagation equation:

$$\frac{\partial P}{\partial x_i} = \frac{P_{perturbed} - P_{nom}}{2\sigma_{x_i}}$$

where:

$P_{perturbed}$ = Value of the PRIME output parameter for the case where PRIME input variable x_i is perturbed

P_{nom} = Best estimate value of PRIME output parameter being analyzed

The PRIME output parameter variance is then calculated using the standard error propagation equation. The 95% confidence values for the output parameter P are given by:

$$P_{95} = P_{nom} \pm K_{95}\sigma_p$$

where:

K_{95} = 95% confidence statistical tolerance factor

= 1.645

The specific parameters perturbed include:

[[

]]

In addition to the parameters above, the statistical analysis methodology includes a model uncertainty perturbation to address fundamental uncertainties in the PRIME qualification results and known product and operation uncertainties. The details relative to how these uncertainties are determined and applied are covered in Section 3 of this report. In general, these uncertainties relate to geometry and material properties for the product and a variety of items related to operation (including oxidation and crud).

1.3.2. Worst Tolerance Analyses

The analysis relative to protecting against exceeding the cladding strain limit is performed using a worst tolerance approach where all design and operating parameters that impact calculated cladding strain are placed at their worst tolerance limit. [[

]]

1.4. OUTLINE OF ANALYSIS

The GNF fuel rod thermal-mechanical design analysis process begins with a specified fuel rod design (nominal parameters and tolerances) and a bounding LHGR limits curve (operating envelope) for analysis per the flow diagram in Figure 1-1 below. The design parameters and limits curve are obtained by integration of operating goals and limitations. [[

Global Nuclear Fuel
A Joint Venture of GE, Toshiba, & Hitachi

]]

[[

]]

Figure 1-1 Flow Chart for Fuel Rod Thermal Mechanical Analysis Using PRIME

The result of these analyses is an LHGR limit curve and steady-state overpower limits which will ensure that the fuel rod will conform with all fuel rod thermal-mechanical design and licensing limits during normal operation, including anticipated operational occurrences.

1.5. IMPLEMENTATION

Upon approval of this LTR, including the application methodology to assure compliance with applicable Reference 1 requirements, GNF will update Reference 1 to include the use of PRIME as an approved method for thermal-mechanical analysis of GNF Fuel Rods to meet fuel rod licensing requirements.

2. *LICENSING REQUIREMENTS*

The limits imposed on calculated fuel rod thermal-mechanical performance are defined to ensure that each fuel rod design satisfies requirements in Sections 1.1.2A and 1.1.2B (i, vi, ix, and x) of Reference 1. The requirements are summarized below in Table 2-1 and discussed in detail below in Section 2.2.

Table 2-1 Fuel Rod Thermal-Mechanical Design Limits

Criterion	Governing Equation
1. The cladding creepout rate ($\dot{\varepsilon}_{CladdingCreepout}$), due to fuel rod internal pressure, shall not exceed the fuel pellet irradiation swelling rate ($\dot{\varepsilon}_{FuelSwelling}$).	$\dot{\varepsilon}_{CladdingCreepout} \leq \dot{\varepsilon}_{PelletSwelling}$
2. The maximum fuel center temperature (T_{center}) shall remain below the fuel melting point (T_{melt}).	$T_{center} < T_{melt}$
3. The cladding circumferential plastic strain ($\dot{\varepsilon}_{\theta}^{P}$) during an overpower transient shall not exceed 1%.	$\dot{\varepsilon}_{\theta}^{P} \leq 1.0\%$
4. The fuel rod cladding fatigue life usage ($\sum_i \frac{n_i}{n_f}$), where n_i = number of applied strain cycles at amplitude ε_i and n_f = number of cycles to failure at amplitude ε_i, shall not exceed the material fatigue capability.	$\sum_i \frac{n_i}{n_f} \leq 1.0$

2.1. BASIS FOR REQUIREMENT

The bases for the thermal-mechanical limits discussed in Section 2.2 below are unchanged from Reference 1, which has been approved by the NRC.

2.2. LICENSING LIMITS

The sections below discuss in detail each of the analysis limits that will be imposed during thermal-mechanical licensing analysis with PRIME. The discussion includes defining the basic parameters used and the analyses results relative to licensing limits.

2.2.1. Fuel Rod Internal Pressure Limit

The outward cladding creep rate due to fuel rod internal pressure during steady-state operation is limited to be no greater than the fuel irradiation swelling rate. This limit is imposed to prevent adverse fuel rod thermal effects postulated to result from late-life opening of the pellet-cladding gap at power. These effects include a positive thermal feedback mechanism leading to higher fuel temperatures and additional fission gas release, which further reduces the pellet-cladding gap conductance and leads to even higher fuel temperatures and additional fission gas release, increased fuel rod internal pressure and higher cladding outward creep rate.

The fuel rod internal pressure for which the cladding outward creep rate is equal to the pellet swelling rate is denoted the critical pressure. A statistical calculation of the critical pressure is made based on statistical fuel rod parameters and operating conditions. The critical pressure and PRIME statistical results for fuel rod internal pressure are used to calculate an internal pressure design ratio. The upper 95% confidence design ratio, as calculated using the statistical internal pressure and the critical pressure, is required to be less than or equal to 1.0.

Specifically, the design ratio is defined by the equation

$$DR_{95} = P_i / \{P_c - 1.645 [\sigma_{pi}^2 + \sigma_{pc}^2]^{0.5} \}$$

where

DR_{95} = lower 95 design ratio
P_i, P_c = nominal internal and critical pressures
σ_{pi}, σ_{pc} = internal and critical pressure standard deviations

The basis for this limit on fuel rod internal pressure has previously been approved by the USNRC as an alternate limit which meets the requirements of paragraph II.A.1(f) of Reference 6. The application for, and approval of, this alternate limit is documented in GESTAR-II (Reference 1).

2.2.2. Overpower to Incipient Fuel Center Melting

This limit is imposed to ensure that fuel failure due to fuel melting does not occur during Anticipated Operational Occurrences (AOOs) resulting from a single operator error or single equipment malfunction. The basis for this limit is derived from paragraphs II.A.2(e) and II.A.2(g) of Reference 3.

[[
]] By requiring this power margin to incipient center melting, the fuel is protected from entering the molten state at the fuel centerline for the anticipated spectrum of AOOs. All fuel rod designs are analyzed to determine the actual minimum (thermal) over-power limits to fuel melting. These limits are utilized during core design and reload activities. The minimum margin has been determined based on the spectrum of slow and fast transients for the BWR fleet. A different target value may be specified for a new design based on knowledge of the design and details of operating conditions and reactor conditions. Each core design is analyzed to ensure that fuel melting will not occur for that specific design and application.

The [[ ]] accounts for changes in gap conductance and fuel temperature due to relaxation of pellet-cladding interaction stresses by cladding creep during a long transient. This time interval addresses the time allowed for the operator to take action to reduce power in case of an event requiring operator action.

2.2.3. Cladding Strain Requirement

After the initial rise to power and the establishment of steady-state operating conditions, the pellet-cladding gap will eventually close due to the combined effects of cladding creepdown, fuel pellet irradiation swelling, and fuel pellet fragment outward relocation. Once hard pellet-cladding contact has occurred, cladding outward diametral deformation can occur. The consequences of this cladding deformation are dependent on the deformation rate (strain rate).

2.2.3.1.High Strain Rate Cladding Strain Requirement

Depending on the extent of irradiation exposure, the magnitude of the power increase, and the final peak power level, the cladding can be rapidly strained due to the fuel pellet thermal expansion occurring during rapid power ramps. This high strain rate deformation can be a combination of (a) plastic deformation during the power increase due to the cladding stress exceeding the cladding

material yield strength, and (b) creep deformation during the elevated power hold time due to creep-assisted relaxation of the high cladding stresses. Such high strain rate cladding permanent (plastic plus creep) deformation due to an AOO is limited to a maximum of 1.0%. The use of a permanent strain limit for fast transients is based on the high strain capabilities of GNF cladding as presented in Reference 7. In particular, GNF fuel cladding has demonstrated capability to at least 2.0% total strain (corresponding to ~1.5% permanent strain).

2.2.3.2.Low Strain Rate Cladding Strain Requirement

During normal steady-state operation, once the cladding has come into hard contact with the fuel, subsequent fuel pellet irradiation swelling causes the cladding to deform gradually outward. The fuel pellet swelling rate is very slow. The effect of this slow fuel pellet expansion is the relaxation of low stresses imposed by the fuel swelling, resulting in a low strain-rate outward creep deformation of the cladding. Similarly, when the fuel rod internal pressure exceeds the external pressure imposed by the reactor coolant, the cladding will also slowly creep outward. Under both of these conditions, irradiated Zircaloy exhibits substantial creep ductility. For example, Ibrahim (Reference 7) reports circumferential tensile creep strains as high as 18% without fracture. For comparison, the imposition of fuel pellet irradiation swelling stresses beginning at the start of irradiation and continuing throughout lifetime to 100 GWd/MTU will result in a low-stress tensile circumferential creep strain of less than 1.8%. Therefore, no specific limit is applied to low-strain rate cladding deformation.

2.2.4. Cladding Fatigue Limit

As a result of power changes during normal operation, cyclic loadings are applied to the fuel rod cladding by the fuel pellet. Therefore, the fuel rod is evaluated to ensure that the cumulative duty from cladding strains due to these cyclic loadings will not exceed the cladding fatigue capability. The Zircaloy fatigue curve employed represents a statistical lower bound to the existing fatigue experimental measurements. The fatigue cycles are counted using the "rainflow" cycle counting method. The limit for fatigue cycling, to assure that the licensing basis is met, is that the value of calculated fatigue usage must be less than the material fatigue capability (fatigue life usage < 1.0).

This limit is imposed to ensure that the cumulative effects of strain cycling during normal operation, including AOO's, will not result in cladding failure. The combined cladding fatigue usage is given by (References 5 and 6)

$$\sum_{j=1}^{2N}\left[\frac{\frac{1}{2}}{N_f}\right]_j \leq 1.0$$

where

j = Cycle j of 2N total strain reversal half cycles during operation.

N_f = the number of cycles to fatigue failure for cladding when subjected to repeated strain increment cycles $\Delta\varepsilon$ which are equal to the strain experienced during one half of cycle j. The strain increase and decrease during cycle j may be different and each half of the strain during cycle j is therefore measured against the material fatigue capability for a summation of the total fatigue duty.

i = index for analysis time increment

n = sum of all PRIME analyzed time increments i with time step greater than zero, including time steps internal to PRIME

3. DESIGN ANALYSIS PROCEDURE

The PRIME methodology utilizes a bounding LHGR envelope to assure compliance with all design and licensing criteria. A thermal-mechanical based LHGR envelope is defined for each fuel rod type and the rod design parameters are specified such that if a rod operates within its specified thermal-mechanical basis envelope of power versus exposure, all design and licensing criteria, including those which address response to anticipated operational transients, are explicitly satisfied, and fuel rod integrity will be maintained.

Fuel rod performance parameters that determine whether the design and licensing criteria are satisfied are fuel centerline temperature, cladding strain and stress, and fuel rod cladding lift-off.

3.1. OVERVIEW OF ANALYSIS PROCEDURE

The PRIME code is utilized in general procedures that are described below in Sections 3.2 through 3.5 to assure compliance with the criteria described above in Sections 2.2.1 through 2.2.4. In all cases that involve statistical analysis, the perturbation procedure summarized in Section 1.2 is utilized to assure (95% confidence) compliance of calculated parameters with corresponding criteria.

3.2. MODEL INPUTS (GENERAL)

This section contains description of the bases of the model inputs for PRIME analyses.

3.2.1. Power History Inputs

The UO_2 rod bounding LHGR operating envelope is derived from nuclear fuel cycle considerations. The envelope is taken to represent operation anticipated by the maximum duty fuel assembly in the central region of the core throughout its operating lifetime. The envelope is defined in terms of LHGR versus peak pellet exposure and generally consists of a period of constant power operation followed by one or more periods during which the power decreases with exposure at a constant rate. A relationship is assumed to exist between the UO_2 and gadolinia fuel rods in the assembly for the purpose of defining gadolinia rod power histories. This relationship reflects the assumption that UO_2 and gadolinia fuel rods in the same fuel assembly will experience similar power histories in terms of time, so that changes in slope of the limits curves will occur at similar exposures and the slopes will be similar. However, the changes in slope will not occur at the same exposure and the slopes will not be identical because gadolinia rods run at different powers and thus accumulate exposure at different rates. Also, the amount of uranium in a fuel rod (per unit weight) decreases with increases in gadolinia concentration. After the exposure dependency of a gadolinia fuel rod is specified on the basis of the UO_2 fuel rod power-exposure history, the maximum power (reduced relative to the UO_2 fuel rod) is specified to ensure compliance with all design and licensing limits.

Thus, the UO_2 and gadolinia fuel rod input power-exposure histories for PRIME analyses are generated using the UO_2 envelope derived from nuclear considerations and reflect planned operation of the rods as well as differences in exposure accumulation due to gadolinia. The histories are input step-wise and

include time increment, the instantaneous power, and cumulative exposure at the peak power axial node of the rod for each time step.

3.2.2. Fuel Rod Axial Power/Exposure/Fluence Distribution

PRIME analyses are performed using 1 or more axial nodes. For multi-node cases, the anticipated axial variations of power, exposure and fluence for a fuel rod are simulated by applying the axial distributions for these parameters to the history discussed in Section 3.2.1. PRIME multi-node analyses generally use 10 axial nodes. The axial power shapes in Table 3-1 for BOC, MOC and EOC simulate the power distribution effects of Burnup Shape Optimization. [[

]] The first set of power distributions shown in Table 3-1 apply to full length UO_2 fuel rods and have a peak/average value of [[ ]]. The second and third sets apply to gadolinia and part length fuel rods, respectively. The axial power, exposure, and fluence distributions for these rods represent the fact that the active fuel lengths for the part length rods differ from the full length UO_2 rod and the active fuel length for the gadolinia rods may differ from the full length UO_2 fuel rod. [[

]]

Table 3-1 Axial Power/Exposure/Fluence Distributions

[[

]]

[[

]]

3.2.3. Fuel Rod Manufacturing Parameters and Operating Conditions

For PRIME statistical analyses, the best estimate and perturbed values of manufacturing parameters are determined from manufacturing specifications. For parameters for which the manufacturing tolerances are symmetric about the nominal specified value, the best estimate value is taken to be the nominal value and the standard deviation is determined by assuming that the manufacturing tolerances encompass two standard deviations on either side of the best estimate value. For parameters for which the manufacturing tolerances are not symmetric about the nominal specified value, the best estimate value is taken to be the nominal value and the standard deviation is determined by assuming that the tolerance band in the direction that produces the worst result is equal to two standard deviations.

The specific methods for specifying PRIME input parameters for the perturbed parameters values are described below.

Global Nuclear Fuel
A Joint Venture of GE, Toshiba, & Hitachi

]]

3.2.4. PRIME Model Uncertainty for Statistical Analysis

The PRIME fuel rod thermal-mechanical performance model has been developed as a best estimate predictor of fuel performance. Verification of the best estimate prediction capability is provided by the extensive experimental qualification in Reference 3. Thus for the PRIME statistical application methodology, only the PRIME model uncertainty is required to be addressed.

[[

]] The basis is discussed below.

3.2.4.1.Power Uncertainty

The PRIME model perturbation is based upon recognition that the fuel rod is a highly thermally driven system. Figure 3-2 presents PRIME centerline temperature qualification results. In Figure 3-2, predicted fuel centerline temperatures are compared to experimentally determined temperatures obtained by direct in-reactor measurement by fuel central thermocouples or expansion thermometers. As indicated by Figure 3-2, the magnitude of the uncertainty in predicted fuel temperatures increases in proportion to the magnitude of the temperature, indicating a constant percentage uncertainty. Since the fuel pellet centerline temperature increase relative to the coolant temperature is directly proportional to the fuel rod power level, a constant percentage uncertainty in fuel temperature is equivalent to a constant percentage uncertainty in effective power level. Statistical analysis of the Figure 3-2 results indicate a standard deviation in temperature, and thus in effective power level, of [[ ]]. The effect of applying a [[ ]] power perturbation on the predicted temperatures in Figure 3-2 is shown in Figure 3-3. These results confirm that the [[ ]] adequately characterizes the PRIME model uncertainty for fuel temperature calculations. In particular, the 2σ perturbation overpredicts 99% of the data.

3.2.4.2.Fission Gas Release Model Perturbation

Figure 3-4, Figure 3-6 and Figure 3-8 present PRIME fission gas release, fuel rod internal pressure, and cladding strain qualification results, respectively. [[

]] The results of the combined perturbation are shown in Figure 3-5, Figure 3-7 and Figure 3-9. These results confirm that the combined [[ ]] perturbation adequately characterize the PRIME model perturbation for fission gas release, rod internal pressure and cladding strain calculations.

3.2.4.3.Model Perturbation for Statistical Analyses

Based upon the results above, the PRIME model perturbation based upon the experimental qualification can be applied by applying a [[ ]] power perturbation and the fission gas release model perturbation. This perturbation addresses the uncertainties in the actual operating power histories for data in the PRIME experimental qualification, as well as uncertainties in fuel and cladding fabrication parameters and in data collection techniques. However, consistent with the use of bounding operating limits, the PRIME methodology explicitly addresses uncertainty in power monitoring in specification of the limits. This uncertainty is characterized as [[ ]] (Reference 10). [[ ]] Also, because the impact of uncertainty in [[

]] in the model uncertainty. These uncertainties are combined with the [[ ]] power uncertainty as follows and included in the PRIME model perturbation.

[[

]]

Thus for statistical analyses, the PRIME model perturbation is taken to consist of a [[
]] model perturbation noted above.

3.3. GENERAL ANALYSIS ASSUMPTIONS

3.3.1. Bounding LHGR Curve

The first step in the fuel rod design and licensing analysis process is to specify maximum operating limits (LHGR limits) for the different fuel rod types. These limits are specified in the form of peak rod local power as a function of the peak pellet exposure in the fuel rod. An example power-exposure envelope is shown in Figure 3-10. This maximum power versus exposure envelope is then used for all fuel rod thermal-mechanical design analyses to evaluate the fuel rod design features and operating conditons and demonstrate conformance to the design and licensing criteria. This maximum (steady-state) power versus exposure envelope is applied as a design constraint to the reference core loading nuclear design and reload core design analyses. This maximum steady-state power versus exposure envelope is also applied to ensure that actual operation is maintained within the fuel rod thermal and mechanical design and licensing bases.

3.3.2. Axial Profiles and Sweeping

The PRIME analyses are conservatively performed assuming that the peak power node of the fuel rod operates on the limiting power-exposure envelope throughout the fuel rod lifetime. The fuel rod axial power shape [[

]] The relative axial power distributions used for a full length fuel rod are presented in Figure 3-11.

3.3.3. Oxide and Crud Inputs

The cladding corrosion and corrosion product (crud) buildup statistical distributions in terms of initial thickness and rate are derived from characterization measurements taken on production fuel rods operating in commercial nuclear reactors. For example, Figure 3-1 shows a comparison of the design corrosion model to the available GNF oxide thickness measurements as determined by eddy current probe lift-off measurements for modern GNF cladding.

---

[1] The major contribution is the PRIME model uncertainty of (See Figure 3-3). Some parameters contributing to the PRIME model uncertainty, in addition to power uncertainty, are[[
]]

3.4. ANALYSIS INPUTS AND ANALYSIS PROCEDURES

The rod internal pressure is determined by the total number of gas atoms for each gas species in the rod free volume. The total number of atoms is the sum of initial helium fill gas atoms and fission gas atoms released from the fuel during operation. Fission gas release is dependent upon the release fraction, which is a function of temperature and exposure, and the total atoms generated, which is a function of exposure. Thus, the rod internal pressure is strongly dependent upon operating history.

3.4.1. Lift-Off Analysis

Fuel rod internal pressure is limited by the licensing requirement that there be no opening of the pellet-cladding gap due to high fuel rod internal pressure at operating power levels. Conformance to this limit is assured by limiting the fuel rod internal pressure to the value for which the cladding creepout rate is equal to the pellet (solid) fission product swelling rate; higher pressure would result in cladding liftoff and gap opening. This pressure is denoted the critical pressure. In GNF licensing analyses, the internal pressure design ratio is used to quantify the internal pressure relative to the critical pressure. The design ratio is determined statistically using calculated distributions of critical pressure and rod internal pressure. For licensing analyses, the design ratio is calculated such that a design ratio of less than 1.0 indicates with at least 95% confidence that the rod internal pressure is less than the critical pressure and thus that the licensing limit is satisfied.

The critical pressure is a function of cladding creepout rate, which in turn is a function of cladding creep properties and cladding thickness and temperature, and pellet swelling rate, which in turn is a function of LHGR. [[

]] in terms of a mean value and standard deviation, as discussed below.

Finally, the internal pressure design ratio is determined statistically using the distributions of critical pressure and rod internal pressure determined as described above. For licensing analyses, the design ratio is calculated statistically such that a design ratio of less than 1.0 indicates with at least 95% confidence that the rod internal pressure is less than the critical pressure and thus that the licensing limit is satisfied The applicable equation for design ratio is found in Section 2.2.1.

$$DR_{95} = P_i / \{P_c - 1.645 [\sigma_{pi}^2 + \sigma_{pc}^2]^{0.5} \}$$

where:

DR_{95} = lower 95 design ratio
P_i, P_c = nominal internal and critical pressures
σ_{pi}, σ_{pc} = internal and critical pressure standard deviations

3.4.1.1.Rod Internal Pressure and Critical Pressure Calculations

Results of PRIME perturbation analyses are utilized to determine the rod internal pressure mean value and standard deviation (P_i and σ_{pi}). Based on values of LHGR, exposure and fluence for each axial node, calculation of these parameters is performed for each axial node and each time step specified by the user. The nodal values of LHGR reflect axial sweeping.

The critical pressure mean value and standard deviation (P_c and σ_{pc}) for each axial node and each time step are determined by solving directly for the internal pressure for which the creep rate is equal to the swelling rate. [[

]]

3.4.2. Fuel Melt Overpower Analysis

The fuel pellet centerline temperature for the maximum duty fuel rod is statistically determined using PRIME. Evaluations are performed for each fuel rod type over a range of exposures and overpowers to simulate various AOOs. The evaluations reflect operation on the bounding power-exposure operating envelope prior to the AOO. Based upon the results of these evaluations, fuel type specific thermal overpower limits are defined to prevent centerline melting. Analyses are performed to determine the values of the maximum overpower (Thermal Overpower) magnitude that does not result in violation of the no fuel (centerline) melting criterion for the 95/95 case. Conformance to the Thermal Overpower criterion is demonstrated as a part of the normal core design and transient analysis process by comparison of the calculated core thermal overpowers, as defined schematically in Figure 3-12, to the thermal overpower limits determined by the PRIME analyses.

3.4.3. Cladding Strain Overpower Analysis (Core Wide Event)

Analyses are performed to determine the values of the maximum overpower (Mechanical Overpower) magnitudes that do not result in the cladding circumferential strain exceeding the 1% cladding permanent strain limit. [[

]]

Conformance to the Mechanical Overpower criterion is demonstrated as a part of the normal core design and transient analysis process by comparison of the calculated core transient mechanical overpowers, as defined schematically in Figure 3-12, to the mechanical overpower limits determined by the PRIME analyses.

[[ ]] The PRIME inputs that impact the results significantly are biased to the fabrication tolerance extreme in the direction that produces the most severe result. Table 3-2 presents the analysis fabrication parameter biases and bases for those biases. Other input parameters conservatively biased for this analysis include (a) cladding corrosion (2σ), and (b) corrosion product (crud) buildup on the cladding outer surface (2σ).

Table 3-2 Worst Tolerance Analysis Manufacturing Parameter Biases

Parameter	Bias Direction	Basis
[[		
		]]

3.4.4. Cladding Fatigue

The cladding fatigue analysis also reflects operation along the maximum steady-state power-exposure envelope. However, superimposed on the power-exposure history are power and coolant pressure/temperature changes. The power change spectrum used is listed in Table 3-3.
The fuel duty cycles shown in Table 3-3 represent conservative assumptions regarding power changes anticipated during normal reactor operation including anticipated operational occurrences, planned surveillance testing, normal control blade maneuvers, shutdowns, and special operating modes such as daily load following. The cladding strain cycles are analyzed using the "rainflow" cycle counting method. The fractional fatigue life expended for each strain cycle is determined and summed over the total number of cycles to determine the total fatigue life expended over the fuel design lifetime. The material fatigue capability is taken as a lower bound to the available experimental measurements of Zircaloy fatigue capability. The statistical calculation determines the mean value and standard deviation of total fatigue life expended. The upper 95% value of fatigue life expended is required to be < 1.00.

3.4.5. Thermal-Mechanical Inputs to Other Analyses

As discussed in Section 1, the PRIME code has been developed to address high exposure phenomena and mechanisms and it is intended to replace the GESTR-Mechanical code in thermal-mechanical analyses. It is also intended to replace the GESTR-LOCA (Reference 9) and GESTR-Mechanical codes in analyses performed to generate inputs for other analyses, including LOCA, core transient and stability analyses. Specifically, it is intended that the PRIME code will replace GESTR-Mechanical and GESTR-LOCA in these applications upon approval of the PRIME code and upon review and approval of such applications by the NRC.

Table 3-3 Fatigue Analysis Power Cycles

Power Cycle, (% Rated)	Frequency, (#/yr.)	Duration
[[		
		]]

[[

]]

Figure 3-1 Cladding Corrosion Model Statistical Parameters

[[

]]

Figure 3-2 Predicted vs Measured Fuel Temperature

[[

]]

Figure 3-3 Predicted vs Measured Fuel Temperature with 2σ Power Perturbation

[[

]]

Figure 3-4 Predicted vs Measured Fission Gas Release

[[

]]

Figure 3-5 Predicted vs Measured Fission Gas Release with 2σ Model Perturbation

[[

]]

Figure 3-6 Predicted vs Measured Fuel Rod Internal Pressure

[[

]]

Figure 3-7 Predicted vs Measured Fuel Rod Internal Pressure with 2σ Model Perturbation

[[

]]

Figure 3-8 Predicted vs Measured Cladding Diameter Strain

[[

]]

Figure 3-9 Predicted vs Measured Cladding Diameter Strain with 2σ Model Perturbation

[[

]]

Figure 3-10 Design Basis Power versus Exposure Envelope (Typical)

[[

]]

Figure 3-11 Axial Power Distributions (Full Length Fuel Rod)

[[

]]

[[

]]

Figure 3-12 Thermal and Mechanical Overpowers (Schematic)

4. REFERENCES

1. General Electric Standard Application for Reactor Fuel, NEDE-24011-P-A-15, September 2005.
2. NEDO-33256 "The PRIME Model for Analysis of Fuel Rod Thermal – Mechanical Performance , Part 1 – Technical Bases", January 2007.
3. NEDO-33257 "The PRIME Model for Analysis of Fuel Rod Thermal – Mechanical Performance , Part 2 – Qualification", January 2007.
4. Letter J.S. Charnley (GE), to R. Lobel (USNRC), "Fuel Property and Performance Model Revisions", MFN- 170-84, December 14, 1984.
5. American National Standard for Light Water Reactors Fuel Assembly Mechanical Design and Evaluation, American Nuclear Society Standards Committee Working Group ANS 57.5, ANSI/ANS-57.5-1981.
6. US Nuclear Regulatory Commission Standard Review Plan 4.2 – Fuel System Design, (USNRC SRP 4.2), NUREG-0800 Rev. 2, July 1981.
7. E. F. Ibrahim, Creep Ductility of Cold-Worked Zr-2.5 w/o Nb and Zircaloy-2 Tubes In-Reactor, Journal of Nuclear Materials, Vol. 96 (1981), pages 297-304.
8. Acceptance Referencing of Licensing Topical Report NEDE-24011-P-A Amendment 7 to Revision 6, GE Standard Application for Reactor Fuel Letter, C. O. Thomas (NRC) to J. S. Charnley (GE), [MFN-036-85] March 1, 1985.
9. GESTR-LOCA-A Model for the Prediction of Fuel Rod Thermal Performance, NEDE-23785-1-PA, (Vol. 1), Revision 1, June 1984.
10. NEDO-33173 "Interim Methods for Constant Pressure and Extended Power Uprate and Maximum Extended Load Line Limit Analysis Plus Applications", LTR, January 2006.